Int J Earth Sci (Geol Rundsch) (2012) 101:429–452
DOI 10.1007/s00531-011-0677-8

ORIGINAL PAPER

Imprints of hydrocarbon-bearing basinal fluids on a karst system: mineralogical and fluid inclusion studies from the Buda Hills, Hungary

Zsófia Poros · Andrea Mindszenty · Ferenc Molnár · Jacques Pironon · Orsolya Győri · Paola Ronchi · Zoltán Szekeres

Received: 8 December 2010 / Accepted: 15 May 2011 / Published online: 10 June 2011

Abstract Calcite veins and related sulphate–sulphide mineralisation are common in the Buda Hills. Also, abundant hypogenic caves are found along fractures filled with these minerals pointing to the fact that young cave-forming fluids migrated along the same fractures as the older mineralising fluids did. The studied vein-filling paragenesis consists of calcite, barite, fluorite and sulphides. The strike of fractures is consistent—NNW–SSE—concluding a latest Early Miocene maximum age for the formation of fracture-filling minerals. Calcite crystals contain coeval primary, hydrocarbon-bearing- and aqueous inclusions indicating that also hydrocarbons have migrated together with the mineralising fluids. Hydrocarbon inclusions are described here for the first time from the Buda Hills. Mixed inclusions, i.e., petroleum with 'water-tail', were also detected, indicating that transcrystalline water migration took place. The coexistence of aqueous and petroleum inclusions permitted to establish the entrapment temperature (80°C) and pressure (85 bar) of the fluid and thus also the thickness of sediments, having been eroded since latest Early Miocene times, was calculated (800 m). Low salinity of the fluids (<1.7 NaCl eq. wt%) implies that hydrocarbon-bearing fluids were diluted by regional karst water. FT-IR investigations revealed that CO_2 and CH_4 are associated with hydrocarbons. Groundwater also contains small amounts of HC and related gases on the basin side even today. Based on the location of the paleo- and recent hydrocarbon indications, identical migration pathways were reconstructed for both systems. Hydrocarbon-bearing fluids are supposed to have migrated north-westward from the basin east to the Buda Hills from the Miocene on.

Keywords Calcite · Petroleum inclusion · Hydrocarbon migration · Miocene · Buda Thermal Karst · Pannonian Basin

Zs. Poros · A. Mindszenty · O. Győri
Department of Physical and Applied Geology, Eötvös Loránd University, Pázmány P. s. 1/c, Budapest 1117, Hungary

Zs. Poros · F. Molnár · O. Győri
Department of Mineralogy, Eötvös Loránd University, Pázmány P. s. 1/c, Budapest 1117, Hungary

J. Pironon
Université de Lorraine, CNRS, G2R Laboratory, BP 70239, 54506 Vandoeuvre-lès-Nancy, France

P. Ronchi
ENI Exploration and Production Division, Via Emilia 1, 20097 San Donato Milanese, Italy

Z. Szekeres
Separation Science Research and Education Laboratory, Eötvös Loránd University, Pázmány P. s. 1/a, Budapest 1117, Hungary

Present Address:
Zs. Poros (✉)
Geological, Geophysical and Space Science Research Group of the Hungarian Academy of Sciences, Pázmány P. s. 1/c, Budapest 1117, Hungary
e-mail: poroszsofi@gmail.com

Introduction: previous research on hydrothermal events and related karst processes of the Buda Hills

The Buda Hills is famous for its extensive hypogenic cave system (sensu Klimchouk 2007; Goldscheider et al. 2010) and abundant actual thermal springs. There are also abundant mineralised veins recognised in this area. Caves often occur along these mineralised fractures. These phenomena suggest that thermal water contribution must have been significant both to the paleofluid and to the recent

fluid systems and also invokes close spatial relationship between the recent and paleofluid migration events.

Precipitates related to the paleothermal water circulation in the Buda Hills have been studied by several authors since the end of the nineteenth century. Those studies focused on the most common vein-filling minerals, i.e., calcite and barite (e.g. Braun 1889; Brummer 1936).

Schréter (1912) suggested that there were two stages of the hydrothermal activity: (1) high-temperature fluid circulation resulting in barite and fluorite precipitation and formation of siliceous veins—from Middle Miocene to Early Pliocene—related to the post-volcanic activity of the volcanism in the Visegrád Mts. located north to the Buda Hills. (2) low-temperature hydrothermal activity—from the Late Pleistocene to Holocene—resulting in the formation of travertines. He also suggested that the water of recent thermal springs were diluted by vadose water. Schafarzik (1921) claimed that there was an additional hydrothermal phase related to the Palaeogene volcanism which produced siliceous cementation.

According to the model of Kovács and Müller (1980), the first fluid circulation event took place under confined conditions. They proposed that the heat source of that fluid flow event was the nearby Neogene volcanism. The second phase—from the latest Miocene—occurred already under unconfined conditions. In this stage, they have already assumed a significant karstic contribution to the thermal water system.

Nádor (1991, 1992) claimed that the first high-temperature fluid circulation resulted in hydrothermal veins. These veins became exposed by younger caves which formed during the subsequent low-temperature fluid circulation event.

Several fluid inclusion studies were carried out on the vein-filling calcite and barite of the Buda Hills (Gatter 1984; Dublyanszky 1991; Molnár and Gatter 1994; Benkovics et al. 1999; Gál et al. 2008). They all showed that their parent fluids were of low salinity (<3 NaCl wt%) and characterised by a wide range of homogenisation temperatures ($T_h \approx$ 50–250°C). Gál et al. (2008) confirmed the suggestion of Báldi and Nagymarosy (1976) regarding the Oligocene age of siliceous cementation of the Oligocene sandstone. They also distinguished a subsequent hydrothermal event of late Early to Middle Miocene age by fitting the orientation of barite veins into the paleostress field model by Márton and Fodor (2003).

Caves of the Buda Karst, hosted mainly by Eocene carbonates, all show fracture-controlled maze-like pattern. Dissolution is explained by the mixing of ascending hydrothermal water and descending meteoric water (e.g. Kovács and Müller 1980; Takács-Bolner and Kraus 1989; Leél-Őssy and Surányi 2003; Erőss et al. 2008). Alföldi (1979) detected hydrocarbon indications in some of the wells in the basin side. He considered it as an evidence for basinal contribution to the karst system.

Our first aim was to decide whether the studied veins from different localities are related to the same regional fluid flow event or not. We also aimed to decide whether the mineralising fluids had direct volcanic connections indeed, or the fluids are rather sourced from the nearby basin. Also we wanted to confirm our statements by quantitative analytical data. In addition, our goal was to establish the possible relationship between the paleo- and recent hydrogeology and thus between the veins and the younger cave systems of the Buda Karst on the basis of reconstruction of the paleofluid migration pathways.

Geology and structural evolution of the Buda Hills

The Buda Hills is located at the north-eastern margin of the Transdanubian Range (TR) in the central part of the Pannonian Basin (Fig. 1). The Pannonian Basin is a Neogene structure formed as a result of extension-related attenuation of the lithosphere in late Early to Late Miocene times (Royden and Horváth 1988). In the latest Miocene, inversion of the basin began and contributed to the uplift of certain blocks. The TR is one of these uplifted blocks. Due to the thin lithosphere, the whole area is characterised, even now, by elevated heat flux (averaging to 100 mW/m^2) as compared to the surrounding regions (Lenkey et al. 2002).

During the Triassic, the TR was part of the shelf of Neotethys located between the South Alpine and East Alpine Units (Haas et al. 1995). In Middle Anisian to Ladinian times, rifting resulted in the opening of intrashelf basins where pelagic limestones and dolomites formed, whereas on the higher elevated blocks shallow-water carbonate sedimentation continued (e.g. Wein 1977). In the Buda Hills, shallow-water carbonate production survived throughout the Carnian and Norian and beyond (represented, e.g. by Hauptdolomit and Dachstein Limestone).

Jurassic and Cretaceous sediments are altogether missing in the area of the Buda Hills. However, since continuous sedimentation prevailed in other parts of the TR from Early Jurassic to early Middle Cretaceous times, we assume that they were also present in the Buda Hills. From Middle Cretaceous on, the TR became involved in thrusting and related flexural deformation (Tari 1994) resulting in subaerial exposure.

The eroded surface of the Triassic sediments is covered by a Palaeogene transgressional sequence at the base with bauxitic clays then with Upper Eocene to Lower Oligocene limestone, marls and clays. In the western part of the Buda Hills, Lower Oligocene sediments are represented by

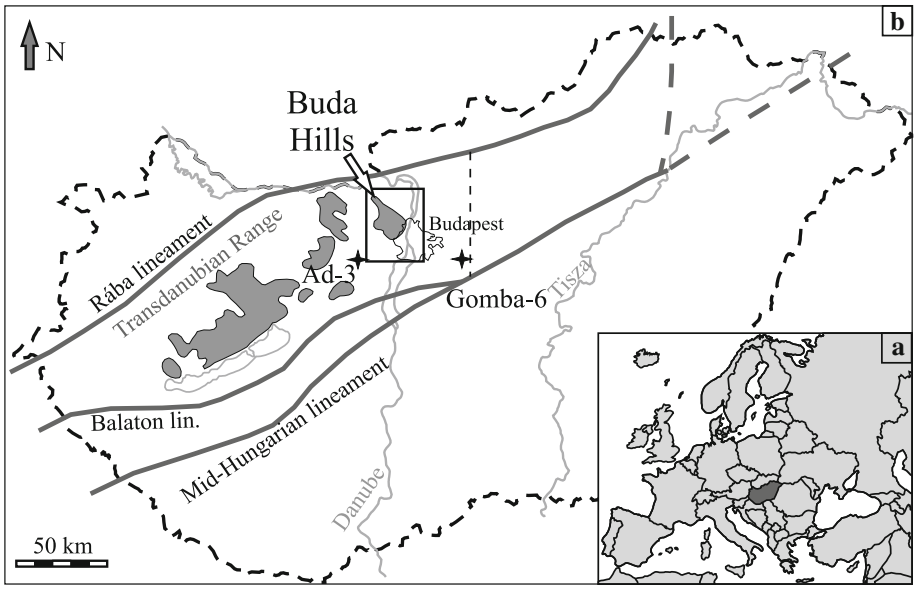

Fig. 1 Location of the Buda Hills

marine, coastal sandstones. The two depositional environments are separated by a prominent structural feature, the Buda Line. Sedimentation continued up to the end of Oligocene represented by shallow marine sandstones. Based on detailed tectonic measurements, Fodor et al. (1994) suggested that from the late Middle Eocene throughout the Oligocene and up to the Early Miocene, the Buda Hills were subject to a stress field resulting in large-scale strike-slip movements.

By Miocene times, the Buda Hills became subaerially exposed and the erosion of Palaeogene rocks initiated. Simultaneously, due to NW–SE trending normal faulting, sedimentation continued in the subsiding basinal sectors and partly also along the margins of the Buda Hills. In the latest Miocene, at certain parts of the Buda Hills, freshwater limestone accumulated on the eroded surface of the Triassic or Eocene formations (Müller and Magyar 2008). From the latest Miocene–Pliocene on, the Buda Hills unit underwent differential uplift and erosion due to compressional tectonics. In Pleistocene times, travertines formed at the margins of the uplifting Hills mainly along NW–SE trending faults. They reflect hydrological changes associated with the uplift since the younger travertines occur at lower topographic positions in comparison with the older ones (Scheuer and Schweitzer 1988).

Applied methods

CL petrography was performed on a MAAS–Nuclide ELM-3 type cold cathode luminoscope on polished thin sections at the Department of Physical and Applied Geology, Eötvös L. University.

Stable carbon and oxygen isotope analyses were carried out in the Institute for Geochemical Research, Hungarian Academy of Sciences. The samples were measured by a Finnigan MAT delta S type mass spectrometer after being pulverised and using the conventional anhydrous phosphoric acid digestion method, under vacuum (McCrea 1950). Isotope compositions are in δ notations as permil deviations from the V-PDB (Vienna Pee Dee Belemnite) carbonate standard. Reproducibility of $\delta^{18}O$ and $\delta^{13}C$ values is better than $\pm 0.2‰$.

Major, trace and rare earth elements were measured by ICP-AES and ICP-MS by a commercial analytical laboratory.

For the fluid inclusion studies, 100-μm-thick, doubly polished thin sections were prepared. Microthermometry was done on a Linkam FTIR 600 heating-freezing stage at the Department of Mineralogy, Eötvös L. University. Standardisation has been carried out on −56.6, 0 and 385°C temperatures using quartz wafers containing synthetic H_2O and H_2O–CO_2 fluid inclusions. Accuracy of the measurements during freezing experiments and heating up to 150°C was 0.1°C.

Bulk composition of petroleum-bearing inclusions was determined by gas chromatography (GC) at the Department of Analytical Chemistry, Eötvös L. University. GC was done by the Agilent 6890N GC 5973 MS using the HP5-MS column. The procession of the sample preparation is the following: few grams of the pulverised mineral was submerged in hexane (C_6H_{14}) and put into an ultrasonic bath, so organic compounds from the decrepitated fluid inclusions could dissolve as much as it is possible. The light fraction of the hydrocarbons ($<C_{10}$) was not detected because it was lost by evaporation during the sample preparation.

Raman analysis was done in doubly polished mineral chips at the Budapest University of Technology and Economics, Hungary. Inclusions were analysed using a Jobin Yvon confocal Labram Raman instrument with 532 nm Nd-YAG laser excitation beam, 20 mW laser energy and 50× objective.

UV epifluorescence was acquired on a Nikon Eclipse microscope equipped with 40× and 60× oil immersion objectives and using Hg light illuminator. The block filter (UV-1A) allowed selection of incident radiation at 365 ± 10 nm, and fluorescence was collected above 400 nm. Photomicrographs were recorded using a numerical camera at G2R laboratory (Nancy Université, France).

Fourier transform-infrared (FT-IR) analysis was done at LEM laboratory (Nancy Université, France). A Bruker IFS 55 Fourier transform spectrometer, coupled with a Bruker microscope, collects the infrared beam with cassegrain objectives (×15). Analysis of petroleum inclusions in thin (i.e. less than 300 μm) doubly polished sections is done by transmission, using a circular diaphragm with a variable diameter aperture (>8 μm), adjusted to the size of the inclusions. Spectral resolution is 4 cm^{-1}, and integration time is longer than 2 min and increases as the inclusion size decreases. Spectra are plotted in absorbance units in the mid-infrared range. A reference spectrum is recorded on the host mineral near the inclusion and subtracted from the inclusion spectrum. Contributions of calcite are removed from the inclusion spectrum when calcite peaks are not oversaturated. The analytical limit is around 1,800 cm^{-1} due to the IR absorption by the host mineral. Spectra of atmospheric CO_2 and H_2O vapours are also subtracted.

Confocal scanning laser microscopy (CSLM) has been applied to petroleum inclusions to record fluorescence images. This is a high resolution imaging technique with an x–y resolution near 0.1 μm and a z resolution near 0.3 μm. CSLM images acquisition has been made on a Biorad Rainbow system adapted to a Nikon inverted microscope at G2R laboratory (Nancy Université, France). A blue diode at 405 nm has been chosen to generate the incident radiation. The fluorescence is collected at wavelengths higher than 420 nm to produce the x–y fluorescence image of 512 × 512 pixels. The objective (60×, oil immersion) moves along the z-axis in order to obtain a series of x–y 8 bit images. The Igor software (©Wavemetrics) and the ImageJ free software are then applied to threshold the images, reconstruct the voxels and then to calculate the volume of the fluorescent liquid oil inside the inclusion. The volume of the gas bubble is approximated to a sphere, and its diameter is measured from the CSLM image recorded by transmission. The gas percentage at room conditions is calculated.

Modelling of petroleum inclusions is based on Peng-Robinson equation of state. It requires T_h and gas vol% as input data. PIT software (Petroleum Inclusion Thermodynamics) produces a P–T diagram with isopleth and isochores and gives a composition estimate with physical properties of the oil (API gravity, GOR; Thiéry et al. 2000, 2002). It uses both (1) the homogenisation temperatures (T_h) measured by microthermometry and (2) the gas bubble filling degree (Fv) measured by CSLM. It is associated with a two-parameter (α, β) compositional model that describes the wide range of compositions of natural hydrocarbon fluids.

Results

Field observations

Calcite-barite-sulphide veins, often with brecciated and cemented zones on both sides (Fig. 3a), hosted by Mesozoic-Tertiary sedimentary rocks are common in the Buda Hills. These veins have been recognised and studied at thirteen localities (Fig. 2) in several host rocks of various lithologies and ages. The mineral association varies by host rock types, e.g., calcite forms wide veins in carbonates (Fig. 3b) and hardly occurs in sandstone. Apart from the sandstones, the only omnipresent phase of the paragenesis is calcite. Since we detected changes in the vein-filling paragenesis by host rock types, the field observations are also described according to their different host rocks.

Vein-filling paragenesis hosted by the Triassic (Ladinian–lower Carnian) Budaörs Dolomite Formation

Abundant calcite veins hosted by the Budaörs Dolomite are exposed mainly in the southern part of the Buda Hills at Odvas Hill and at Törökugrató quarry (Fig. 2). The bulk of these hills is made up by the Budaörs Dolomite partly covered by Eocene sediments.

At the Odvas Hill, the dolomite is of mosaic breccia texture and more intense brecciation occurs along single fractures and fracture zones. Calcite cementation occurs along these zones, resulting in prominent erosion-carved zones (Fig. 3c). There are also simple calcite veins without any breccia clasts. The strike of both the simple veins and the breccia veins is mainly NNW–SSE. In the central part of the calcite veins, there is often some remaining open porosity. Barite and limonite were also detected in minor amounts. Barite frequently occurs together with calcite as well, filling thin fractures where the barite is the older phase. The white, rarely greenish-coloured barite is of bladed habit (Fig. 3d), of a few mm size.

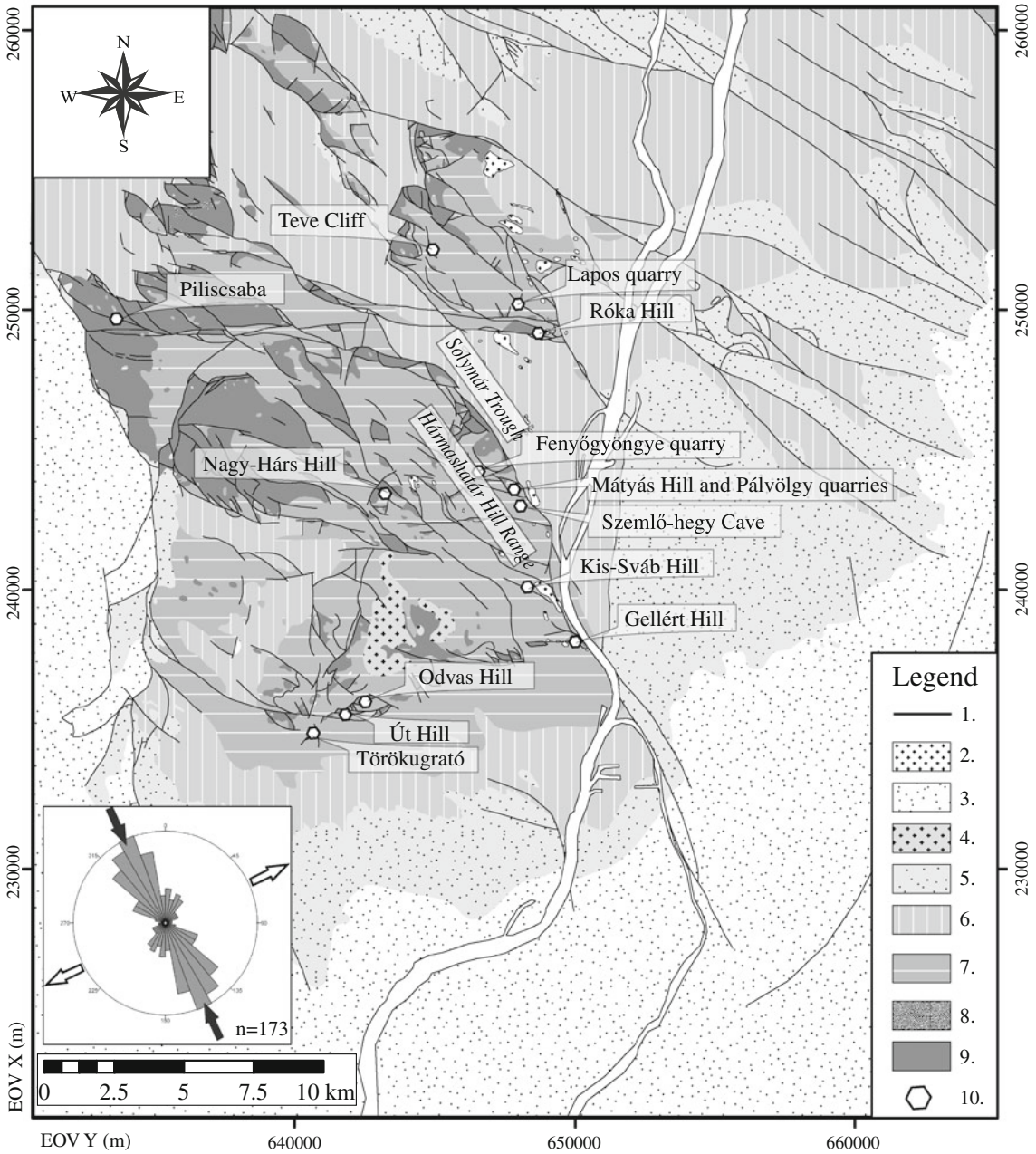

Fig. 2 Studied locations indicated on the pre-Pliocene geological map of the Buda Hills supplemented with Pleistocene travertines, modified after Fodor (unpublished). *1* Structural elements, *2* Pleistocene travertine, *3* Upper Miocene siliciclastics, *4* Upper Miocene freshwater limestone, *5* Lower and Middle Miocene siliciclastics, *6* Upper Oligocene siliciclastics, *7* Upper Eocene to Lower Oligocene carbonates and siliciclastics, *8* Eocene (?) bauxitic clay, *9* Triassic carbonates, *10* Studied locations. *Rose diagram* shows the orientation of calcite veins from all the investigated localities. *Black arrows* show the direction of the maximum compression (σ_1)

At Törökugrató quarry, the Budaörs Dolomite and the Upper Eocene–Lower Oligocene Buda Marl are exposed. Both are crosscut by veins mainly filled with calcite. The thickness of the calcite veins may reach 50 cm. Calcite is coarse-grained and of scalenohedral habit (Fig. 3e). Small (<few mm), colourless hexahedrons of fluorite (Fig. 3f) were found in association with the scalenohedral calcite. Bladed barite similar to that of the Odvas Hill was found in the Triassic dolomite, precipitated prior to the calcite. In the central part of thick calcite veins, where there is still some remaining porosity, scalenohedra show usually corroded surface covered by a younger calcite of cauliflower-like morphology. The cauliflower phase probably precipitated on the walls of a former cave.

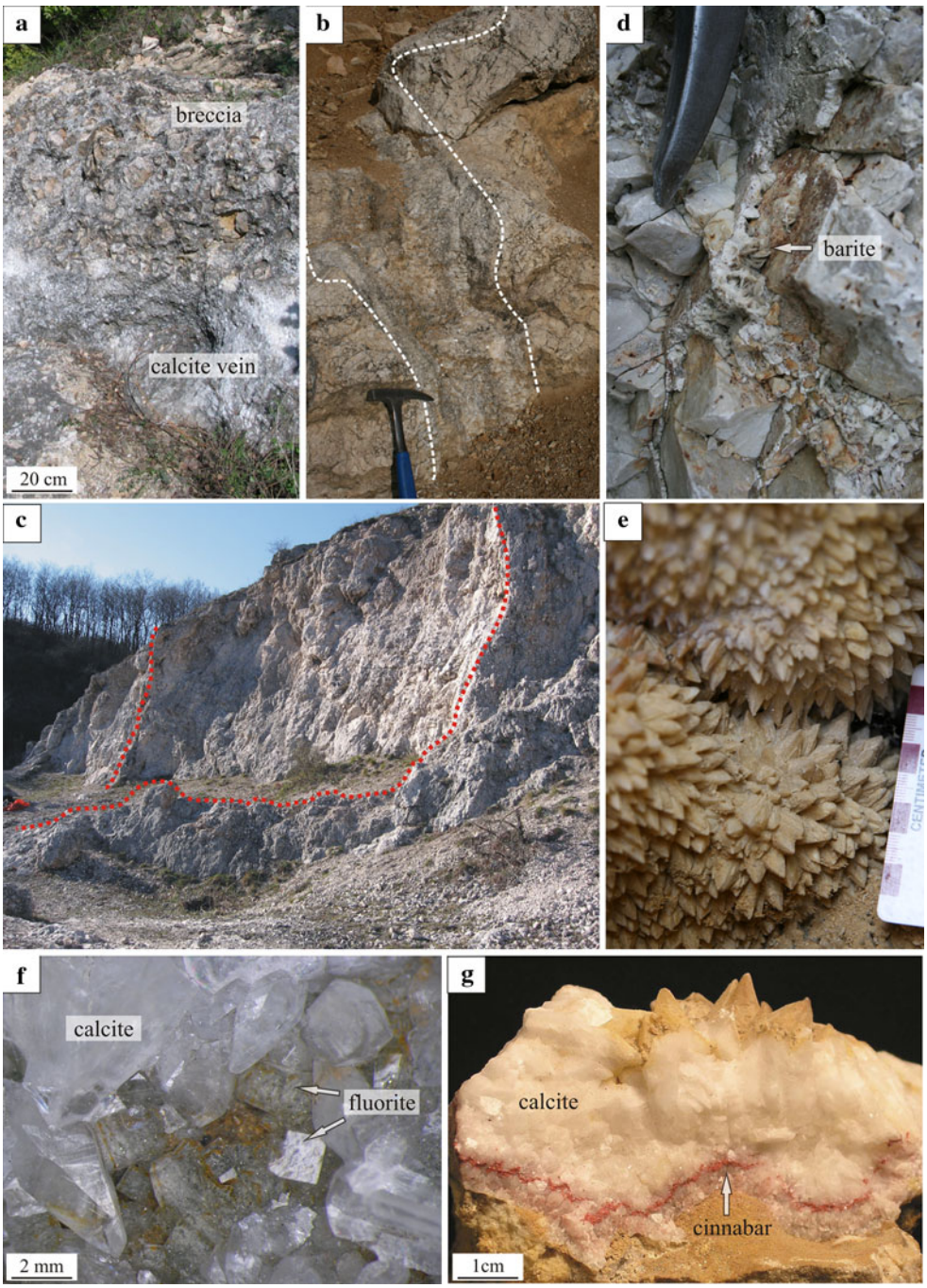

Fig. 3 **a** Calcite vein bordered by calcite-cemented breccia zones; Fenyőgyöngye quarry, **b** Half-metre-wide calcite vein hosted by Triassic Dachstein Limestone; Róka Hill, **c** Dolomite breccia cemented by bladed barite; Odvas Hill, **d** Calcite-cemented breccia zones marked by red dotted lines in the fragmented Budaörs Dolomite; Odvas Hill quarry, **e** Scalenohedral calcite at Törökugrató, **f** colourless, euhedral fluorite crystals between calcite scalenohedra; Gellért Hill, **g** Calcite with cinnabar from the Róka Hill

Vein-filling paragenesis hosted by the Triassic (Middle (?) Carnian–Norian) Hauptdolomit Formation

The Hauptdolomit is well exposed on the Gellért Hill where it is partly covered by Eocene sediments (Fig. 2). The hill is bordered by a normal-dextral fault of Pliocene age from the east (Fodor et al. 1994). Dolomite is crosscut by calcite veins of a few centimetre widths. Minor amounts of fluorite (Fig. 3f) and sulphide (pyrite, marcasite) were also detected in those veins. Moreover, the overlying cherty sandstone is barite-cemented and silicified. The barite has tabular habit and yellowish colour.

Teve Cliff is located in the north-eastern part of the Buda Hills (Fig. 2). Triassic Hauptdolomit is overlain here

by Oligocene sandstone. Some fractures, filled with barite and limonite, occur in the partly disintegrated dolomite. Barite crystals have tabular morphology. These fractures can also be traced in the overlying sandstone which proves their post-Oligocene age.

Only a minor amount of calcite was found in the northwesternmost part of the Buda Hills (south to Piliscsaba; Fig. 2), cementing thin fractures of the dolomite.

Vein-filling paragenesis hosted by the Triassic (Norian–Rhaetian) Dachstein Limestone Formation

In the Róka Hill quarry (Fig. 2), abundant calcite veins are exposed. They are hosted by the Triassic Dachstein Limestone and by the overlying Eocene basal sediments. In the Triassic limestone, there are some half-metre-wide calcite veins with calcite-cemented breccia zones on both sides. Calcite usually has scalenohedral habit. The orientation of veins is uniformly NNW–SSE. There is a 3-m-wide breccia zone (consisting of Triassic and Eocene clasts) which is bordered by a fault, cemented by calcite, towards the Dachstein Limestone. Calcite occurs together with cinnabar, metacinnabar (Nagy and Pelikán 1976) and pyrite. The first phase of the vein-filling calcite is greyish and is usually followed by milky white calcite. In some cases, a cinnabar layer also occurs between these two calcite phases (Fig. 3g). Yellowish, tabular barite of 0.5–1 cm size is also present as a post-calcite precipitation.

In the Nagy-Hárs Hill quarry (Fig. 2), the Dachstein Limestone is overlain by Eocene and Oligocene sediments. The limestone is crosscut by a breccia zone and simple fractures cemented by circumgranular calcite of elongated or scalenohedral habit.

Vein-filling paragenesis hosted by the Eocene (-lower Oligocene) carbonates

There are several outcrops of Eocene limestones (Szépvölgy Limestone) and marls (Buda Marl) in the Hármashatár Hill Range (Fig. 2), which is bordered from the east by a normal-dextral fault of Miocene age (Fodor et al. 1994). These veins are also exposed within the fracture-related caves (e.g. Szemlőhegy Cave, Ferenchegy Cave). This paragenesis was investigated in more detail in the Szemlőhegy Cave and in several outcrops on the surface within the Hármashatár Hill Range and also in the northern part of the Buda Hills at Lapos quarry (Fig. 2).

Almost identical parageneses and phenomena were observed at the following localities: Mátyás Hill , Pálvölgy , Fenyőgyöngye and Lapos quarries. In these localities, calcite fills up to half-metre-wide veins. Wide breccia zones were often found on both sides of the calcite veins. The habit of the calcite crystals is elongated scalenohedral in most of the cases but other morphological types (short scalenohedral, rombohedral and combination of the two) were also distinguished. The greatest morphological variability was observed in Lapos quarry where calcite cemented the brecciated marl. Calcite is accompanied here by tabular barite which is younger than the calcite. A limonitic phase, with few fresh sulphide grains (pyrite/marcasite), was usually observed as a phase preceding the precipitation of calcite (Fig. 4a). These veins have peculiar green-stained patches in the Pálvölgy quarry related to the presence of minor amounts of native copper being oxidised on the actual surface (Lóránth 2000). Few mm wide faded halos were also observed along single calcite veins hosted by reddish-coloured parts of the marl at Lapos quarry (Fig. 4b). Calcite-dominated veins uniformly show NNW–SSE, and subordinately, N–S strike at all the studied localities.

Szemlőhegy Cave exposes a similar vein-filling paragenesis consisting predominantly of calcite. This cave also exposes stylolites filled with black asphalt-like bitumen (Fig. 4c). (Presence of organic matter, e.g. normal alkanes, was proved by GC). Calcite shows scalenohedral habit with the crystals grown in open space (Fig. 4d). Later corrosion and dissolution commonly occur along these veins, resulting in cavities along former calcite veins (Fig. 4e). Orientation of the veins, and also the orientation of the cave corridors, is mainly NE–SW referring to the NE–SW striking right-lateral strike-slip fault (Benkovics et al. 1999). Subordinately, NW–SE striking veins are also present perpendicular to the main strike of the cave. Barite veins were also detected along this latter direction. Fractures alternately filled with calcite and barite were also observed. Similar phenomenon also occurs in the Kis-Sváb Hill hosted by the Eocene marl. In most cases, the first precipitate is calcite of smaller crystal size followed by a yellowish-coloured barite of tabular habit and then a coarse sparry calcite (Fig. 4f). Simple barite veins are also present, consisting of large (up to 3 cm) yellow orthorhombic crystals.

At Út Hill (Fig. 2) the fractures of the Eocene marl are filled with small bladed barite crystals and a small amount of calcite.

Vein-filling paragenesis hosted by Oligocene sandstone in the northern part of the Buda Hills

Hydrothermal phenomena of the Oligocene Hárshegy Sandstone Formation were investigated in more detail by Gál et al. (2008). They detected minerals related to both the Palaeogene and the Neogene hydrothermal systems, the former represented by chalcedony veins. Neogene mineralising fluids apparently migrated along the NNW–SSE striking fractures. Along them, significant amounts of

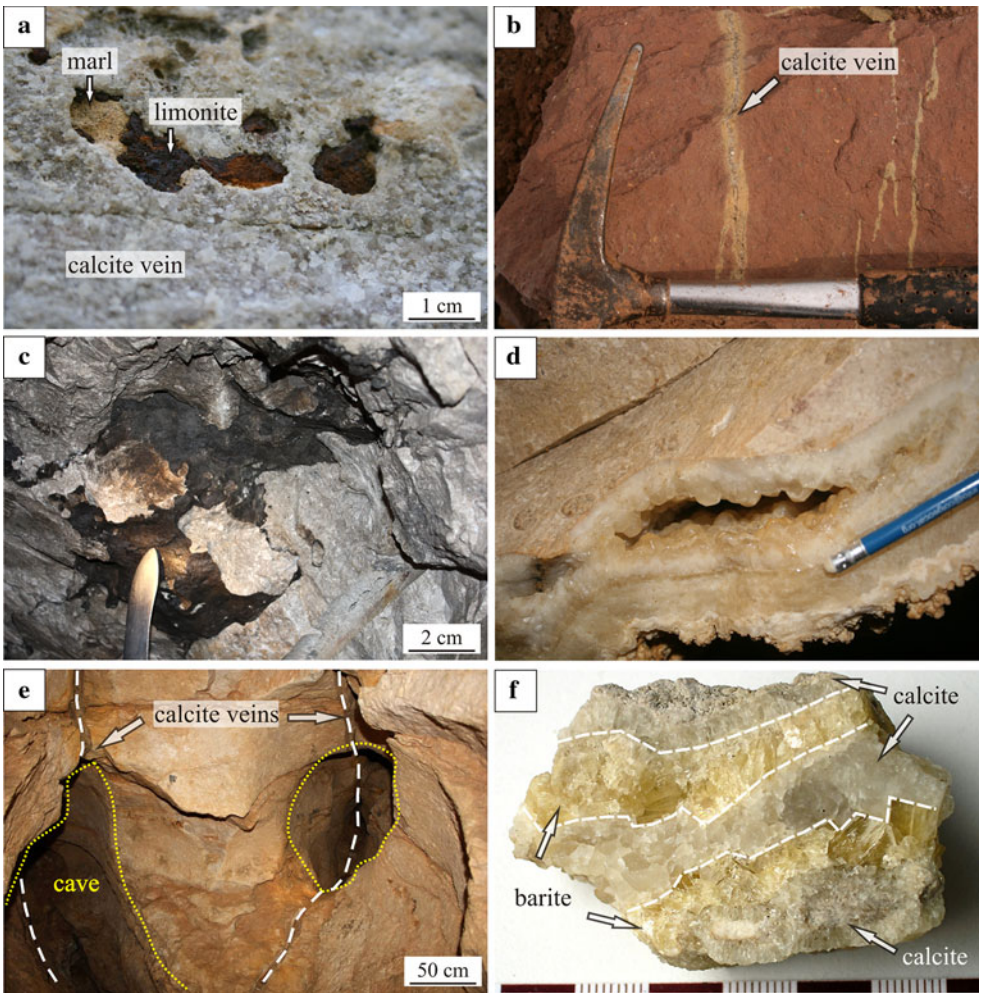

Fig. 4 **a** Limonite predates calcite, hosted by the Buda Marl at Mátyás Hill, **b** calcite veins with faded halo in reddish-coloured Buda Marl at Lapos quarry, **c** stylolite filled with asphalt-like bitumen in the Eocene limestone exposed in the Szemlőhegy Cave, **d** remaining porosity in the central part of a calcite vein in the Eocene limestone exposed in the Szemlőhegy Cave, **e** Cave passages formed along fractures formerly filled with calcite, Szemlőhegy Cave **f** fracture alternately filled with calcite and barite (Kis-Sváb Hill)

barite of various habits occur. Small amount of calcite was also observed together with barite, rarely.

On the basis of the field observations, the following general paragenetic order was established (Fig. 11):

Limonite is commonly hosted in Eocene carbonates in the central and northern part of the Buda Hills (e.g. Pálvölgy quarry, Lapos quarry). This phase is probably the oxidation product of a former iron sulphide (pyrite/marcasite). *Native copper*, described by Lóránth (2000), may be related to this first fracture-filling phase.

Barite-I bladed habit, greenish barite which is mainly present in the Triassic Budaörs Dolomite (and in the Buda Marl). Subordinately, barite-I was also found in the northernmost part of the Buda Hills hosted in the Oligocene sandstone. Both limonite and barite-I predate calcite; however, the relative timing of these two phases is ambiguous since they do not occur together.

Fluorite colourless hexahedrons in between calcite scalenohedra occurring mainly in the southern part of the Buda Hills (e.g. Törökugrató quarry, Gellért Hill).

Calcite omnipresent phase in each locality and each rock types (excluding the sandstone). It gives the largest proportion of the fracture-filling phases. It usually has scalenohedral habit; however, various morphological types were also observed mainly in breccia zones.

Cinnabar, *metacinnabar and pyrite* found intergrown with calcite indicate coprecipitation of these phases. Cinnabar and metacinnabar were found only at Róka Hill.

Barite-II tabular yellowish barite of various crystal sizes (from 0.5 cm up to 3 cm). This phase occurs mainly in the central and northern part of the Buda Hills, most commonly overgrown on calcite, hosted by Eocene carbonates. Alternation of calcite and barite-II was also observed in a few cases (e.g. Kis-Sváb Hill).

At all localities, the strike of extensional fractures filled with the above minerals is uniformly NNW–SSE and subordinately N–S (Fig. 2).

Micropetrography

Fresh *marcasite* was detected along the margins of a calcite vein in the Lapos quarry. Scattered remnants of marcasite were detected in the *limonite* phase, too, which implies that this phase was originally marcasite (Fig. 11).

Bladed barite (*barite-I*) shows growth zoning under stereomicroscope: it has a cloudy, non-transparent central part and a clear rim. This zoning is due to the uneven distribution of abundant fluid inclusions.

Fluorite usually occurs together with calcite and commonly forms aggregates, consisting of small (~few mm) hexahedral crystals. Fluorite usually contains solid inclusions (supposedly calcite grains) along its growth zones in the outer part of the crystals. Euhedral fluorite was also found in calcite as solid inclusions, mainly along growth zones of calcite or as scattered crystal aggregates (Fig. 5a). The presence of fluorite was confirmed by Raman spectroscopy. Fluorite inclusions were commonly detected in calcite of several localities (e.g. Róka Hill, Szemlőhegy Cave, Lapos quarry); thus, fluorite is almost omnipresent within this paragenesis.

Uniform characteristics were observed in the *calcite* from different localities: (1) thick 'spongy' growth zones characterised by abundant fluid inclusions and (2) abundant fluorite inclusions. Cathodoluminescent pattern is uniform as well, showing fine zoning by alternation of thin bright and dull-luminescent or non-luminescent zones (Fig. 5b). Subordinately, sector zoning (Fig. 5c, d) was also observed in calcite veins from Róka Hill quarry. Staining of thin sections revealed the elevated iron content in the core of the calcite crystals.

Fresh and partly oxidised euhedral *pyrite* grains in zones intergrown with calcite.

In addition to the morphological differences of the two barite phases, micropetrographical differences were also found: *barite-II* shows no zoning; it is uniformly clear and contains only minor amounts of mainly one-phase and rarely two-phase (liquid–vapour) fluid inclusions.

Fluid inclusion study

Microthermometry was done on primary fluid inclusions of calcite from three different localities, i.e., Róka Hill, Lapos quarry and Fenyőgyöngye quarry. Primary fluid inclusions showed uniform characteristics in all studied samples but abundant petroleum inclusions were found coeval with aqueous inclusions in the samples from the Róka Hill only. Therefore, detailed description is based on the observations of the samples from this locality. Petroleum inclusion-rich calcite samples were all taken from the boundary of the host rock (Triassic Dachstein Limestone) and vein (Fig. 3b), but petroleum inclusions also occurred subordinately in the central part of the veins. A number of primary, petroleum-bearing inclusions were also found in vein calcite at Fenyőgyöngye quarry (hosted by Eocene limestone) and in a quarry near to Piliscsaba (hosted by Triassic dolomite).

Fluid inclusion petrography

The following three types of primary inclusions were detected based on micropetrography: (1) aqueous inclusions, (2) petroleum inclusions and (3) the mixture of the two: aqueous-petroleum-bearing inclusions.

Aqueous inclusions Aqueous inclusions commonly form thick 'spongy' growth zones (Fig. 5f) in which both intact and decrepitated inclusions can be found. Fluid inclusions generally consisting of liquid and vapour phases with visually determined L:V ratios around 80:20, but rarely some one-phase (L) inclusions also occur. Shape of the inclusions is usually elongated and subordinately necking-down texture also occurs. Outline of all aqueous inclusions is always irregular. The size of the inclusions varies between 10 and 50 μm.

Petroleum inclusions Two-phase (Liquid HC + Vapour HC) inclusions either occur within the same growth zones with aqueous inclusions (Fig. 5h) or form thick growth zones without aqueous inclusions, characterised by extraordinary abundance of the petroleum inclusions (Fig. 5g). Contour of petroleum inclusions are generally sharp but the wall of the inclusion is rarely rough. It was also observed that the contour of the inclusions is sharp on one side and rough on the other side (Fig. 5k). Although petroleum inclusions are commonly rounded, various morphologies were observed by using the CSLM. Fluorescence colour changes as a function of the size of the oil inclusion (Fig. 5e). The most common small (d = 10–20 μm) yellow-coloured inclusions show bright bluish-white fluorescence colour (Fig. 5i, j). Green and red fluorescence colours were also observed in larger dark brown inclusions (~50 μm) characterised by larger vapour phases. In addition, non-fluorescent layer was detected between two fluorescent immiscible liquid petroleum phases within certain inclusions. Three-dimensional images, obtained by using CSLM, pointed out that these inclusions do not contain different immiscible liquid phases, only they look like to do so (Fig. 6). This phenomenon is due to the peculiar shape of the inclusions. Using CSLM, it is also possible to measure the L/V ratio. In this case, the

volume of the vapour phase (Fv) was around 5% in the case of smaller inclusions where leakage is less likely.

Aqueous-petroleum-bearing inclusions Subordinately, mixed-type inclusions were also found consisting of aqueous and petroleum phases within one and the same inclusion: Liquid HC + Vapour HC + Liquid H_2O ± Vapour H_2O. In this case, the proportion of the aqueous and petroleum phases is widely variable. Mixed-type inclusions most commonly consist of a two-phase (L-V) oil drop with a one-phase (L) 'water-tail' (Fig. 7a). Rarely mixed-type inclusions were observed containing two immiscible vapour phases. Moreover, it was also observed that the 'water-tail' already came off the oil drop represented by an elongated one-phase inclusion located just near by a two-phase rounded oil inclusion.

Secondary, generally one-phase and rarely two-phase aqueous inclusions were also observed along healed microfractures. They were not the target of investigation since our aim was to establish the physical and chemical properties of the fluid from which the calcite precipitated.

Microthermometry

Microthermometry was done on the coexistent two-phase aqueous and petroleum inclusions. Both aqueous and petroleum inclusions homogenised into the liquid phase in each cases. While homogenisation temperature is restricted to a narrow interval, between 78 and 88°C, in the case of petroleum inclusions, those of the aqueous inclusions fall into a much wider interval from 80°C up to 114°C (Table 1). However, it has to be noted that these intervals overlap and show similar minimum values.

Final melting temperatures of ice were measured in the case of aqueous inclusions. Salinities calculated from the ice-melting temperature values vary between 0.4 and 0.9 NaCl eq. wt%, assuming H_2O–NaCl system, and there is only one outstanding value at 3 NaCl eq. wt%. Final melting temperature was higher than 0°C in two particular cases, probably due to the metastable melting of ice (Table 1). We could not detect the eutectic temperature of the aqueous inclusions in any cases; therefore, we assume NaCl-bearing fluids to be enclosed by calcite.

Microthermometry was also used on two-phase aqueous inclusions in calcite not occurring together with petroleum inclusions. Fluid inclusion petrography of these aqueous inclusions is similar to those accompanied by oil inclusions. Both homogenisation temperature (T_h = 70–280°C) and salinity data (0–1.7 NaCl eq. wt%) overlap from the three different localities (Róka Hill, Lapos quarry, Fenyőgyöngye quarry). Nevertheless, there is an outstanding salinity value of 2.6 NaCl eq. wt% from the Róka Hill (Fig. 11).

FT-IR analysis

FT-IR was used to determine the composition of individual hydrocarbon-bearing inclusions since this method is more efficient in the case of hydrocarbon-bearing inclusions than Raman spectroscopy because it is not affected by fluorescence (Pironon et al. 2000). We used the FT-IR instead of Raman analysis also in the case of aqueous components of the inclusions because the host calcite was fluorescent, too. Liquid and vapour phases were measured separately, at room temperature, in the case of large (>50 μm) petroleum inclusions. Three simple two-phase (L_{HC} + V_{HC}) hydrocarbon-bearing inclusions were investigated by FT-IR. No significant differences were detected in different inclusions. However, CO_2 content varies from 0 to 4 mole% and CH_4 from 3 to 15 mole% (Table 2). Methane concentration is higher in the vapour phase, while CO_2 is rather related to the liquid phase in dissolved form. CH_2/CH_3 ratio varies from 5 to 8.5 corresponding to equivalent nC_{12} to nC_{19}, respectively. None of the two-phase oil inclusions contain detectable amount of water. One mixed-type oil inclusion with 'water-tail' was also measured by IR. Although the composition of the hydrocarbon phase shows great similarity with those of the simple two-phase oil inclusions, this inclusion contains large amounts of CO_2 (in the vapour phase and dissolved in oil) but gas fractions cannot be determined because of the saturation of the IR spectrum in the C–H stretching range due to the large size of the inclusion and the thickness of the host mineral (absorption of overtones of carbonate groups superimposed to –CH contributions). Furthermore, the aqueous phase (=water-tail) of this peculiar inclusion also contains CO_2 besides water (Fig. 7b). No high amount of methane was detected in this inclusion. Thus, the aqueous phase may represent the H_2O–NaCl ± CO_2 system. Therefore, the calculated salinity values represent the maximum salinity of the fluid because the invisible amount of CO_2 may reduce the final melting temperature by maximum 1.5°C (Hedenquist and Henley 1985). Thus, the outstanding salinity value (3 NaCl

Fig. 5 Micropetrographic observations on the vein-filling calcite ▶ **a** Euhedral fluorite inclusions in calcite (sample from Szemlőhegy Cave) **b** fine CL zoning of calcite (sample from Mátyás Hill) **c** sector zoning in calcite from the margin of the vein. Cathodoluminescent image **d** petroleum inclusions along a growth zone of calcite. Transmitted light **e** same picture under UV light **c**–**e** same calcite crystal **f** spongy growth zones consisting of decrepitated and intact aqueous fluid inclusions in calcite **g** abundant petroleum inclusions in the core of the calcite crystal and fluorite inclusions along the adjoining growth zone **h** coeval, two-phase (L-V) aqueous and petroleum inclusions within the same growth zone **i**–**k** well-rounded petroleum inclusions **i** transmitted light **j** UV light **k** 3D image obtained by CSLM of a petroleum inclusion with well-rounded contour on one side and rough on the other side **c**–**k** sample Ro-13, Róka Hill (Fig. 3b)

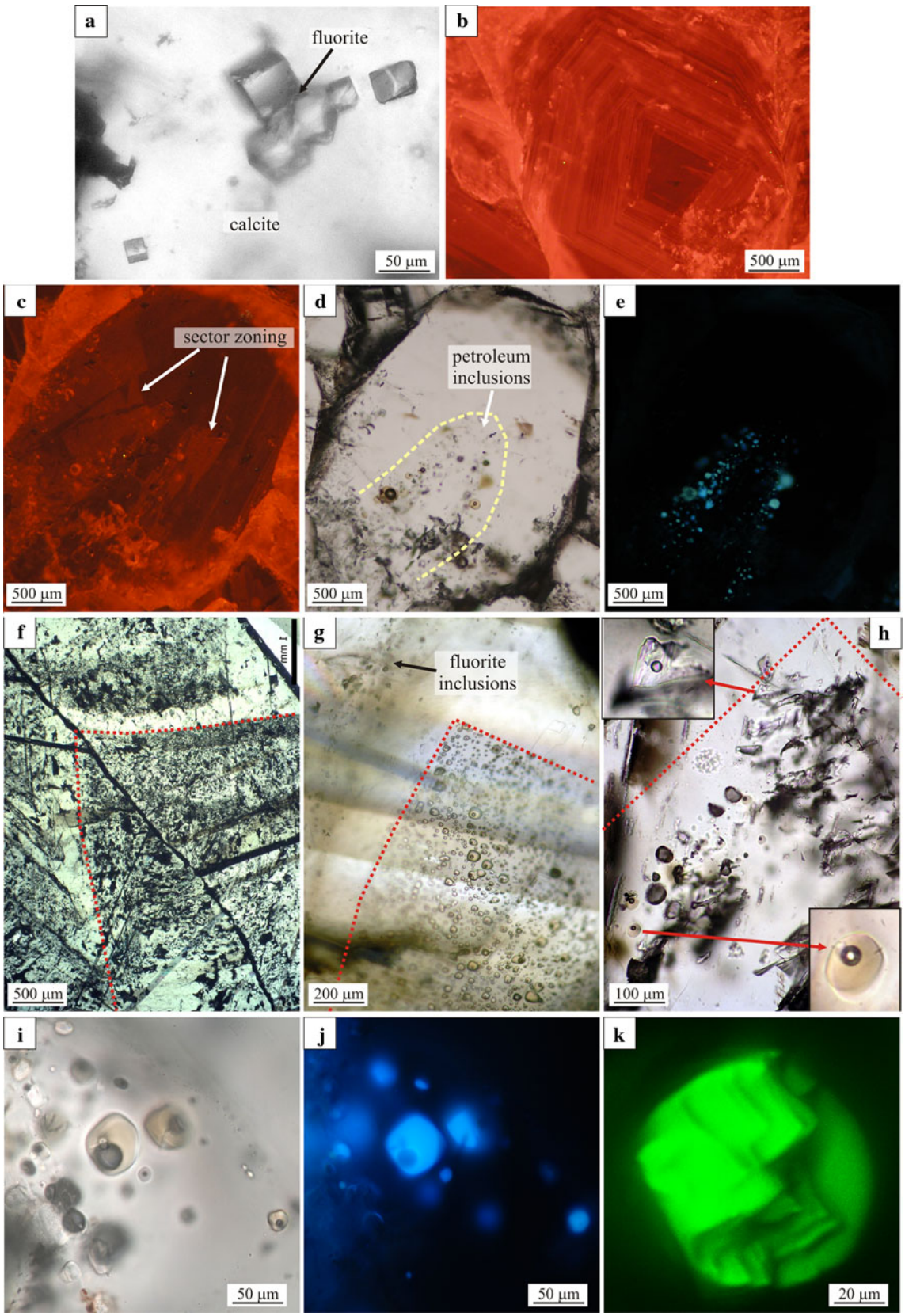
a
fluorite
calcite
50 µm
b
500 µm
c
sector zoning
500 µm
d
petroleum
inclusions
500 µm
e
500 µm
f
500 µm
g
fluorite
inclusions
200 µm
h
100 µm
i
50 µm
j
50 µm
k
20 µm

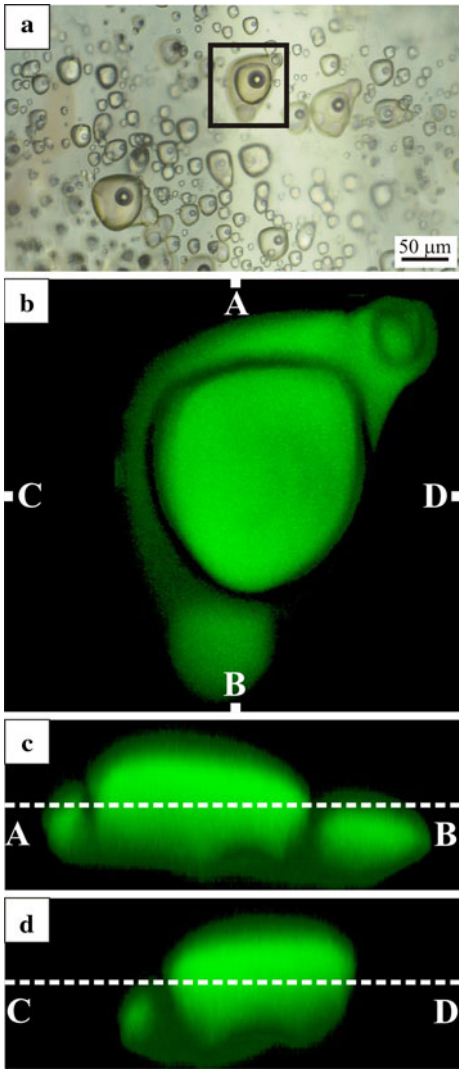

Fig. 6 Petroleum inclusions of peculiar shape. Note that they look like having more than two immiscible phases **a** transmitted light **b–d** 3D images obtained by using CSLM from three different views

wt%) may be related to an inclusion containing CO_2 because the depression of the final melting temperature is just about 1.5°C higher as compared to the average value (−0.3°C) of all data (Table 1).

Gas chromatography

Gas chromatography (GC) was used to establish the bulk composition of petroleum enclosed in the calcite. The most frequent normal alkane compounds are of carbon atomic number between 17 and 24. There is a hump, representing the unresolved complex mixtures, around C_{30} on the gas chromatogram (Fig. 12). Besides the normal alkanes, we also identified two isoprenoids, namely pristane and phytane, by their positions relative to nC_{17} and nC_{18}, respectively. Presence of these isoprenoids was confirmed by GC–MS. Using the PIT software, it is possible to calculate the composition of individual petroleum inclusions from the following input data: homogenisation temperature and measured L/V ratio (Thiéry et al. 2000). The result of the calculation by PIT (Table 3) is in accordance with bulk composition of the oil obtained by GC and corresponds to the range given by FT-IR. All methods pointed out that the hydrocarbons, entrapped in the studied calcite, consist of mainly heavy hydrocarbon molecules. However, the highest frequency of HC molecules in individual inclusions is present within the interval of nC_{11} to nC_{19} which is slightly lighter than the bulk composition determined by GC. This may be explained by the fact that when using the GC we underestimate the light fraction of the oil due to the evaporation during the sample preparation.

Geochemistry

Carbon and oxygen isotopes of vein calcite

Based on field observations, we hypothesised that calcite samples from different localities showing uniform characteristics were of the same origin. Stable oxygen and carbon isotopes were measured from vein calcite from numerous localities and from different host rocks in order to confirm the above hypothesis.

Stable isotope values of calcite are well separated from those of the host rocks in each case (Fig. 8). Oxygen isotopes of vein calcite fall into a wide interval (from −9.2 to −18.7‰ V-PDB) depleted as compared to the host rocks (from 1.3 to −9.8‰ V-PDB) (Table 4). No significant differences in the interval of stable isotope values of different calcite veins could be detected. Ranges are broadly overlapping for different localities. There are only three data-points characterised by negative carbon isotope composition; however, significant dissolution was observed on the crystal surfaces in two of the three cases.

Major and trace elements of calcite

Both major and trace elements were measured from ten calcite vein samples from seven different localities. Regarding the major elements, no remarkable differences were observed in calcite samples. Fe_2O_3 content is ranging between 0.1 and 0.3%. Sr concentrations are more variable within the interval from 79.4 to 459 ppm (Table 5). All calcite samples have the same flat rare earth element (REE) pattern, and all of them are depleted as compared to the REE concentrations of PAAS (Post-Archean Australian Shale). However, calcite samples containing HC inclusions are characterised by the lowest REE concentration values. Most REE were below detection limit in the case of the sample containing abundant petroleum inclusions (Fig. 9).

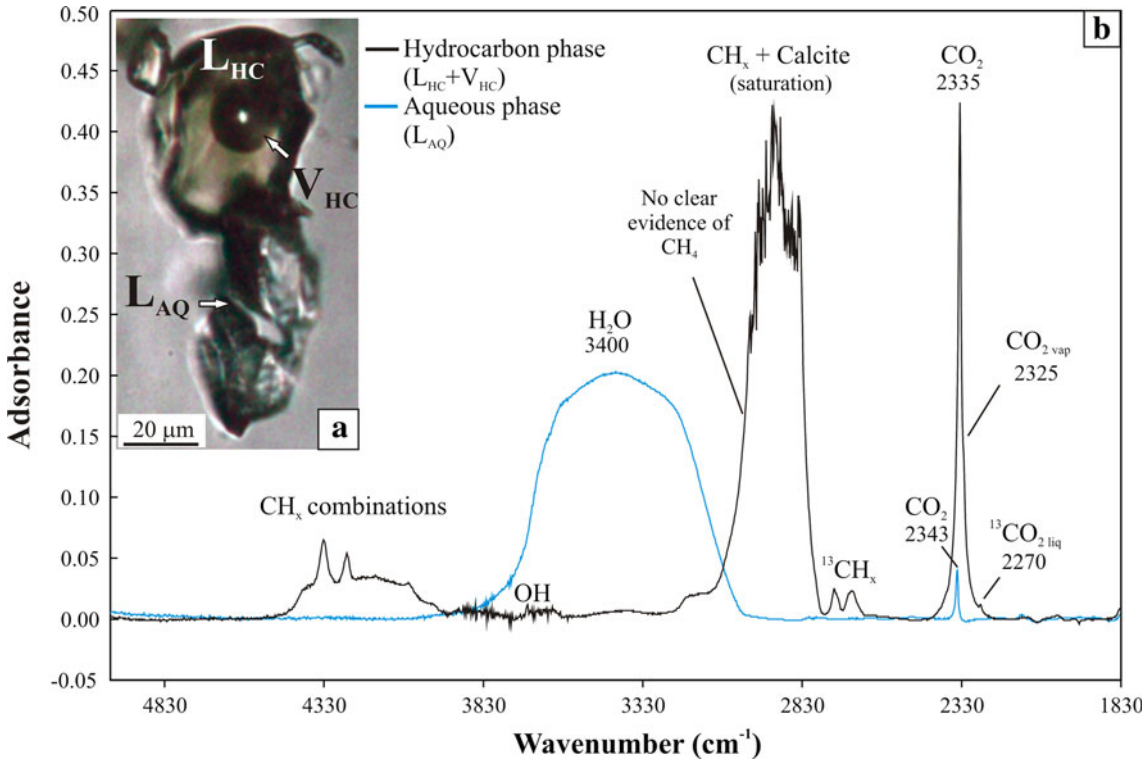

Fig. 7 **a** Mixed-type inclusion in the sample Ro-13/2 (inclusion No. 3) consisting of oil drop and 'water-tail' **b** IR spectrum of the above fluid inclusion

Table 1 Fluid inclusion data of primary coexistent aqueous and petroleum inclusions occurring in the calcite sample Ro-13

Phases	T_h (°C)	T_{melt} (°C)	Salinity (NaCl eq. wt%)	Remarks
Liquid–vapour	99.0			a
Liquid–vapour	80.1			a
Liquid–vapour		−0.3	0.5	b
Liquid–vapour	86.0			a
Liquid–vapour	92.0	−1.8	3.1	a
Liquid–vapour		−0.5	0.9	b
Liquid–vapour	114.0	+0.2		c
Liquid–vapour	113.0	+0.5		c
Liquid–vapour	94.0			a
Liquid–vapour	85.0			a
Liquid–vapour	85.0	−0.2	0.4	
Liquid-vapour	85.0	−0.2	0.4	
Liquid–vapour	93.0	−0.3	0.5	
Liquid–vapour	87.0	−0.2	0.4	

	T_h (°C) min	T_h (°C) max	T_h (°C) mean	Remarks
Aqueous inclusions	80.1	114	92.8	$n = 12$
Petroleum inclusions (L-V)	78.0	88.0	83.2	$n = 27$

[a] The vapour phase of the inclusions disappeared during homogenisation and did not reappear during cooling down to room temperature; therefore, the final melting temperature was not measured

[b] Texture shows necking-down hence only the final melting temperature was measured in this case

[c] No final melting temperature data obtained because of the metastable melting of ice above 0°C

Table 2 Composition of individual petroleum-bearing inclusions obtained by IR

Sample	Inclusion	Measured phase	[CH_4] mole%	[CO_2] mole%	[Alk] mole%	CH_2/CH_3
Ro-13/2	1	Vapour HC	30.0	0.0	70.0	8.6
Ro-13/2	1	Liquid HC	13.8	0.3	85.9	6.4
Ro-13/2	1	Liquid HC (margin of the FI)	16.4	0.1	83.5	4.9
Ro-13/2	2	Bulk (L + V) HC	3.9	2.6	93.4	6.2
Ro-13/3	4	Bulk (L + V) HC	15.4	4.0	80.5	6.0
Ro-13/3	4	Vapour HC	22.8	3.1	74.1	5.6
Ro-13/3	4	Liquid HC	13.5	4.0	82.6	6.2

Table 3 Composition of a representative petroleum inclusion (same inclusion on Fig. 6) calculated by PIT software using the homogenisation temperature (T_h) measured by microthermometry and the gas bubble filling degree (Fv) measured by CSLM

T_h	82.0°C
Fv	5.3%
Tfv	21.0°C
Alpha	0.93
Beta	0.32
Component	Mole %
CO_2	4.0
C_1	19.6
C_2	3.6
C_3	4.5
iC_4	1.2
nC_4	2.6
iC_5	1.9
nC_5	3.1
nC_6	4.5
nC_7	4.8
nC_8	4.6
nC_9	4.4
nC_{10}	4.1
Cn_1	25.6
Cn_2	11.6

Discussion

The studied calcite veins and the related paragenesis from the different localities all belong to the same regional fluid migration event, based on the following uniform properties detected in the case of the omnipresent calcite:

1. Orientation of veins, supposedly extensional in origin, is uniformly NNW–SSE at all the different localities.
2. Appearance of the calcite crystals is also uniform (generally it has scalenohedral habit and milky colour interrupted by growth zones of greyish colour).
3. Vein-filling paragenesis shows great similarities at different localities. For example, calcite is usually accompanied by barite and fluorite. Nevertheless, minor changes of the paragenesis were detected in different host rocks.
4. Geochemical similarities—detected by several analytical methods, i.e., stable isotope geochemistry, fluid inclusion study, trace elements, cathodoluminescence—confirm the uniform origin of vein-filling minerals throughout the Buda Hills.

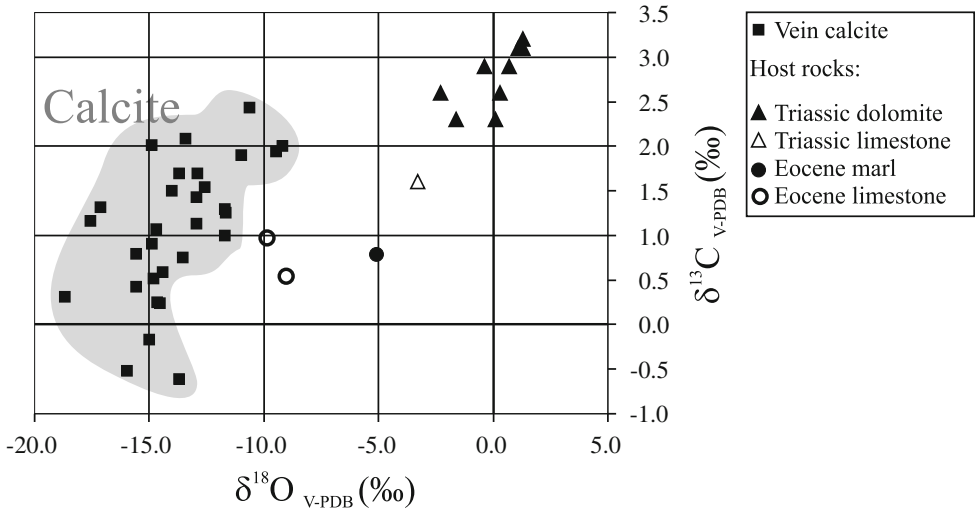

Fig. 8 Stable oxygen and carbon isotope values of calcite veins and of different types of host rocks

Table 4 Stable oxygen and carbon isotope values of vein calcite and different host rocks

Sample code	Sample location and host rock type	Measured phase	δ^{13} C$_{V\text{-}PDB}$ (‰)	δ^{18} O$_{V\text{-}PDB}$ (‰)
O-02	Odvas Hill, Budaörs Dolomite	Dolomite cement	2.3	−1.6
O-02	Odvas Hill, Budaörs Dolomite	Matrix dolomite	2.3	0.1
O-02	Odvas Hill, Budaörs Dolomite	Dolomite cement	2.6	0.3
O-04	Odvas Hill, Budaörs Dolomite	Bulk rock	2.6	−2.3
O-04	Odvas Hill, Budaörs Dolomite	Bulk rock	2.9	−0.4
T-04	Teve Cliff, Hauptdolomit	Dolomite cement	2.9	0.7
T-04	Teve Cliff, Hauptdolomit	Matrix dolomite	3.1	1.3
T-04	Teve Cliff, Hauptdolomit	Bulk rock	3.2	1.3
T-05	Teve Cliff, Hauptdolomit	Matrix dolomite	3.1	1.1
Ro-42	Róka Hill, Dachsten Limestone	Bulk rock	1.60	−3.30
L-17	Lapos quarry, Buda Marl	Bulk rock	0.80	−5.10
F-24	Fenyőgyöngye quarry, Szépvölgy Limestone	Bulk rock	0.56	−8.96
M-14	Mátyás Hill, Szépvölgy Limestone	Bulk rock	0.98	−9.80
L-11	Lapos quarry, Buda Marl	Vein calcite	1.0	−11.7
L-11	Lapos quarry, Buda Marl	Vein calcite	1.3	−11.7
L-05	Lapos quarry, Buda Marl	Vein calcite	2.4	−10.6
L-28	Lapos quarry, Buda Marl	Vein calcite	0.5	−14.8
L-31	Lapos quarry, Buda Marl	Vein calcite	1.5	−12.6
Ro-33	Róka Hill, boundary of breccia and Dachstein Limestone	Vein calcite	1.9	−11.0
Ro-34	Róka Hill, boundary of breccia and Dachstein Limestone	Vein calcite	2.0	−9.2
Ro-35	Róka Hill, breccia	Vein calcite	1.7	−13.7
Ro-24	Róka Hill, Dachstein Limestone	Vein calcite	2.1	−13.4
Ro-46	Róka Hill, breccia	Vein calcite	0.8	−13.6
Ro-20	Róka Hill, breccia	Vein calcite	0.8	−15.6
Ro-61	Róka Hill, breccia	Vein calcite	0.4	−15.6
F-11	Fenyőgyöngye quarry, Szépvölgy Limestone	Vein calcite	1.7	−12.9
F-12	Fenyőgyöngye quarry, Szépvölgy Limestone	Vein calcite	1.5	−14.0
F-05	Fenyőgyöngye quarry, Szépvölgy Limestone	Vein calcite	2.0	−14.9
O-16	Odvas Hill, Budaörs Dolomite	Vein calcite	−0.2	−15.0
O-04	Odvas Hill, Budaörs Dolomite	Vein calcite	0.9	−14.8
Tug-06	Törökugrató, Budaörs Dolomite	Vein calcite	0.6	−14.4
Tug-08	Törökugrató, Budaörs Dolomite	Vein calcite	1.1	−14.7
Tug-08	Törökugrató, Budaörs Dolomite	Vein calcite	1.3	−11.7
Tug-09	Törökugrató, Szépvölgy Limestone	Vein calcite	1.4	−12.9
Tug-03	Törökugrató, Budaörs Dolomite	Vein calcite	0.3	−18.7
Tug-01	Törökugrató, Budaörs Dolomite	Vein calcite (corroded)	−0.5	−16.0
Szb-02	Szemlőhegy Cave, Szépvölgy Limestone	Vein calcite	1.3	−17.1
Szb-11	Szemlőhegy Cave, Szépvölgy Limestone	Vein calcite	1.1	−12.9
Sz-f 1a	Szemlőhegy Cave, Szépvölgy Limestone	Vein calcite (corroded)	−0.6	−13.7
Sz-f 1b	Szemlőhegy Cave, Szépvölgy Limestone	Vein calcite (corroded)	1.2	−17.6
Sz-f 1c	Szemlőhegy Cave, Szépvölgy Limestone	Vein calcite (corroded)	0.2	−14.5
Szb-18	Szemlőhegy Cave, Szépvölgy Limestone	Vein calcite (corroded)	0.2	−14.7
P-15	Piliscsaba, Hauptdolomit	Vein calcite	1.9	−9.5

Physical and chemical properties of mineralising fluids and related hydrocarbons

Based on the stable isotope values, calcite must have precipitated at high temperature because oxygen isotope values, which vary as a function of the temperature (Craig 1965), are always significantly depleted in vein calcite samples. Major and trace element concentrations also suggest elevated temperature for the parent fluid. For example, Tullborg et al. (2008) suggest that high-temperature

Table 5 Concentration of major and trace elements in the vein calcite

	Detection limit	O-16	Tug-01	Tug-03	Szb-11	Szb-18	L-18	Ro-12	M-31	M-29	F-16
SiO_2 (wt%)	0.01	0.09	0.09	0.06	0.13	1.25	0.08	0.12	0.11	0.23	0.03
Al_2O_3	0.01	0.02	0.02	0.01	0.03	0.22	0.03	0.02	0.03	0.06	0.02
Fe_2O_3	0.01	0.02	0.02	0.01	0.03	0.02	0.03	0.01	0.02	0.02	0.01
CaO	0.01	54.3	55.3	55.4	54.7	53.9	55	54.2	53.6	53.5	54.6
MgO	0.01	0.82	0.21	0.22	0.21	0.36	0.13	0.5	0.15	0.89	0.39
Na_2O	0.01	0.02	0.01	0.01	0.02	0.03	0.02	0.03	0.02	0.01	0.01
K_2O	0.01	0.02	0.02	0.02	0.02	0.03	0.02	0.02	0.01	0.02	0.01
TiO_2	0.01	b.d.l.	b.d.l.	b.d.l.	b.d.l.	0.01	b.d.l.	b.d.l.	b.d.l.	b.d.l.	b.d.l.
MnO	0.01	0.08	0.06	0.05	0.02	0.03	0.02	0.01	0.02	0.04	0.02
P_2O_5	0.01	0.01	0.01	0.01	0.01	0.01	0.01	0.01	0.01	0.01	0.01
LOI	0.01	43.1	42.8	42.5	43.2	42.4	43.2	43.3	45.2	43.2	43.2
Total	0.01	98.5	98.6	98.3	98.4	98.5	98.5	98.3	99.2	98	98.4
La (ppm)	0.5	1.4	2.0	1.7	1.0	5.7	0.8	b.d.l.	1.8	1.7	0.8
Ce	0.5	3.4	4.5	3.5	1.6	7.8	1.3	0.5	3.1	2.5	0.8
Pr	0.03	0.47	0.72	0.59	0.25	1.18	0.17	0.06	0.52	0.36	0.13
Nd	0.1	2.0	3.0	2.7	1.1	4.7	0.7	0.2	2.4	1.6	0.6
Sm	0.03	0.42	0.91	0.86	0.25	1.01	0.17	0.04	0.63	0.38	0.15
Eu	0.03	0.12	0.29	0.24	0.06	0.27	0.03	b.d.l.	0.16	0.10	0.04
Gd	0.05	0.43	1.22	1.08	0.32	1.16	0.17	b.d.l.	0.71	0.52	0.20
Tb	0.01	0.07	0.23	0.19	0.05	0.20	0.03	b.d.l.	0.11	0.08	0.03
Dy	0.05	0.4	1.38	1.19	0.26	1.17	0.16	b.d.l.	0.69	0.53	0.17
Ho	0.01	0.08	0.31	0.23	0.05	0.25	0.03	0.01	0.13	0.12	0.04
Er	0.03	0.20	0.84	0.64	0.16	0.78	0.1	b.d.l.	0.35	0.39	0.10
Tm	0.01	b.d.l.	0.10	0.05	b.d.l.	0.07	b.d.l.	b.d.l.	0.02	0.02	b.d.l.
Yb	0.03	0.17	0.62	0.49	0.10	0.65	0.09	b.d.l.	0.29	0.33	0.05
Lu	0.01	0.01	0.12	0.07	0.02	0.1	0.02	b.d.l.	0.04	0.06	b.d.l.
Ba	0.5	54.4	7.2	1.9	61.6	2390.0	2.7	1.5	45.3	21.1	6.0
Co	0.5	0.6	1.2	0.7	1.1	6.4	0.8	0.8	1.8	b.d.l.	2.0
Cs	0.01	b.d.l.	0.13	b.d.l.	0.02	0.09	0.02	b.d.l.	0.01	0.06	b.d.l.
Cu	5	b.d.l.	b.d.l.	b.d.l.	b.d.l.	b.d.l.	b.d.l.	b.d.l.	b.d.l.	b.d.l.	b.d.l.
Ga	0.1	0.1	0.3	0.1	0.1	0.2	0.1	b.d.l.	0.1	0.2	0.1
Hf	0.2	b.d.l.	b.d.l.	b.d.l.	b.d.l.	b.d.l.	b.d.l.	b.d.l.	b.d.l.	b.d.l.	b.d.l.
Ni	5	b.d.l.	b.d.l.	b.d.l.	b.d.l.	b.d.l.	b.d.l.	b.d.l.	b.d.l.	b.d.l.	b.d.l.
Nb	0.2	b.d.l.	0.2	b.d.l.	b.d.l.	b.d.l.	b.d.l.	b.d.l.	b.d.l.	b.d.l.	b.d.l.
Pb	5	b.d.l.	b.d.l.	b.d.l.	b.d.l.	b.d.l.	b.d.l.	b.d.l.	5	6	b.d.l.
Rb	0.2	0.4	0.3	b.d.l.	0.2	0.6	0.2	0.2	b.d.l.	0.3	b.d.l.
Sr	0.1	243.0	194.0	164.0	108.5	231.0	79.4	288.0	86.9	459.0	429.0
Ta	0.1	b.d.l.	0.1	b.d.l.	b.d.l.	b.d.l.	b.d.l.	b.d.l.	b.d.l.	b.d.l.	b.d.l.
Th	0.05	0.46	0.37	0.12	0.12	0.40	0.08	0.07	0.14	0.08	b.d.l.
U	0.05	0.40	1.67	0.58	0.13	0.19	0.29	b.d.l.	0.32	0.07	b.d.l.
V	5	5	15	14	b.d.l.	11	b.d.l.	b.d.l.	b.d.l.	9	b.d.l.
W	1	3	3	3	2	4	4	7	2	2	3
Y	0.5	2.8	10.1	9.6	2.2	11.7	1.8	b.d.l.	5.1	5.1	2.0
Zn	5	b.d.l.	12	b.d.l.	b.d.l.	18	b.d.l.	b.d.l.	b.d.l.	b.d.l.	b.d.l.
Zr	2	3	3	2	3	6	5	3	3	3	4

Letters of sample codes indicate: *O* Odvas Hill, *Tug* Törökugrató, *Szb* Szemlőhegy Cave, *L* Lapos quarry, *Ro* Róka Hill, *M* Mátyás Hill, *F* Fenyőgyöngye. *b.d.l.* below detection limit

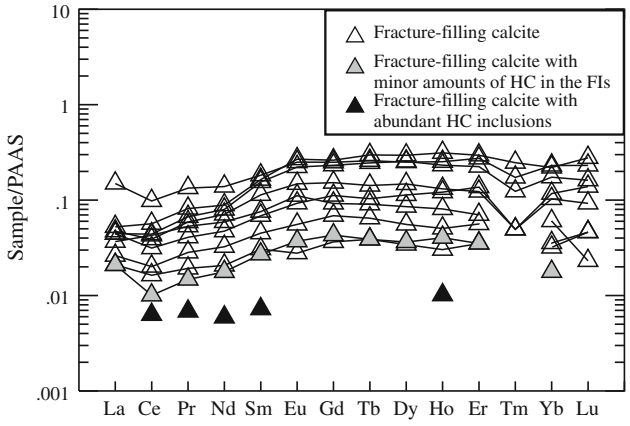

Fig. 9 REE pattern of different vein calcites from different localities [normalised data for Post-Arch. Aust. Shale (PAAS) REE, Taylor and McLennan (1985)]. Missing data points are below the detection limit

(~150°C) fracture-filling calcites are characterised by elevated Sr contents (>100 ppm). Fracture-filling calcites from the Buda Hills (with 80–460 ppm Sr) fall within this range. Nevertheless, elevated Sr content may be also explained by the source of fluids. If the source of this fluid was rich in Sr, more Sr would be incorporated in the calcite. A question could be raised whether this calcite is of hydrothermal origin in the sense that it precipitated under conditions considerably warmer than the surrounding host rocks at that time.

Fluid inclusion petrography of calcite suggests a heterogeneous parent fluid consisting of dilute water and an immiscible hydrocarbon phase and that both inhomogeneous and homogeneous entrapment occurred. Furthermore, the peculiar well-rounded shape of the oil inclusions occurring together with elongated aqueous inclusions suggests that petroleum and water may have been entrapped together and then they separated and the resulting two different inclusions consist of predominantly water and petroleum, respectively. This process can be interpreted as a transcrystalline migration of the enclosed water by dissolution and later recrystallisation of the wall of the inclusion triggered by the thermal gradient as it was first

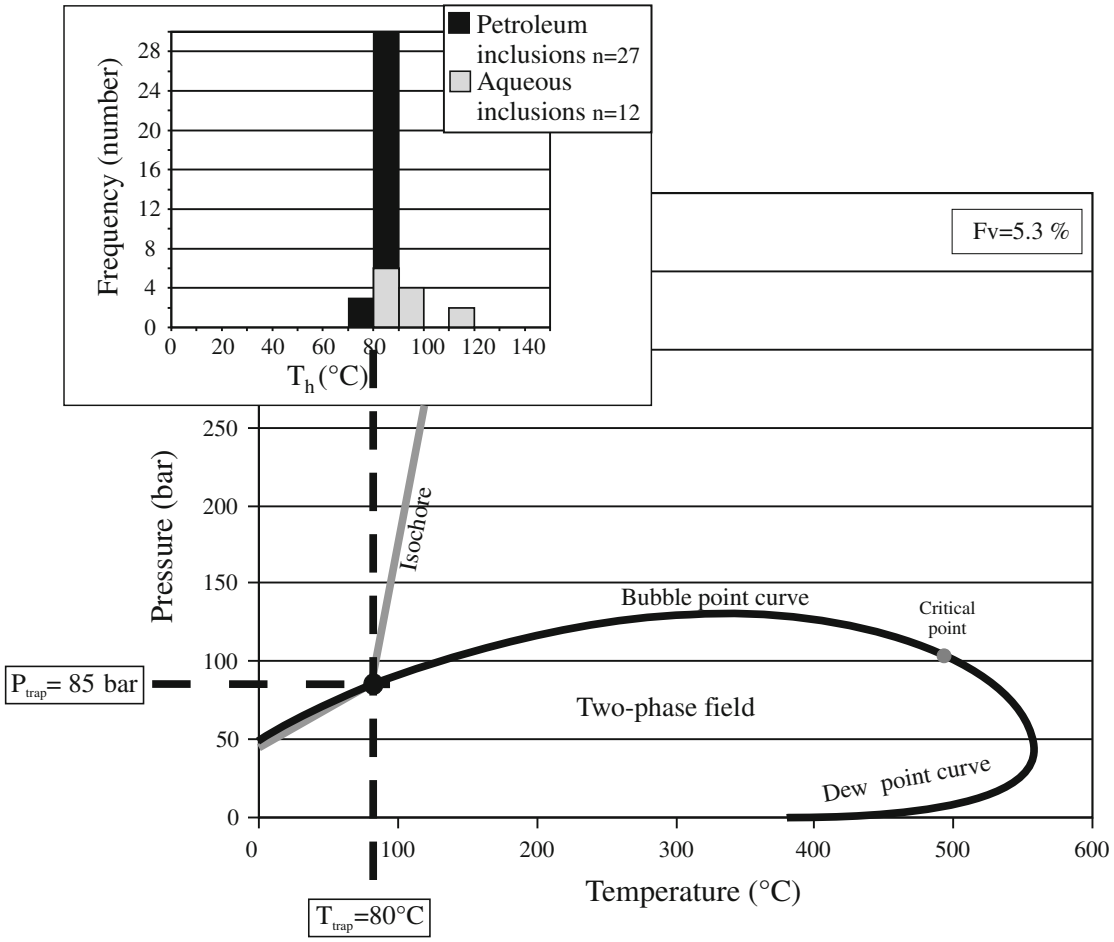

Fig. 10 Pressure and temperature conditions during entrapment of coeval aqueous and petroleum inclusions in calcite calculated by PIT software (Róka Hill, sample Ro-13)

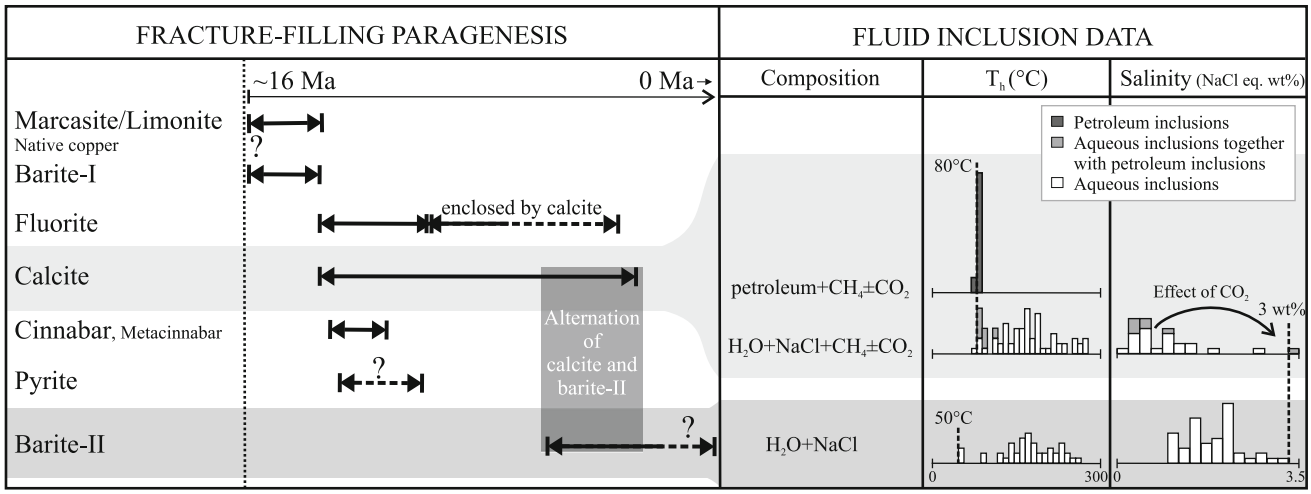

Fig. 11 Paragenetic order of fracture-filling minerals and the related fluid inclusion data. Fluid inclusion data of barite-II are from Gál et al. (2008)

described by Lemmlein (1952) in the case of salt crystals. Intense thermal water migration along the veins may have provided the sufficient thermal gradient in our case. While inclusions in salt crystals move towards the heat source, we assume a migration to the opposite direction in our case because of the retrograde solubility of calcite. Nevertheless, it has to be noted that the separation of water and petroleum was not complete in each cases. The mixed-type inclusions with 'water-tail' (Fig. 7a) may represent an intermediate stage of this process. In the case of contemporaneous trapping of two immiscible fluids from a heterogeneous system, the homogenisation temperature of the aqueous phase represents the trapping temperature for both fluids (Nedkvitne et al. 1993), so pressure correction must not be undertaken (Burruss 1981). Thus, the minimum value of the homogenisation temperatures of our aqueous inclusions (~80°C) has to be taken into account (both for aqueous inclusions occurring together with petroleum inclusions and for those without), supposing a volume change of certain inclusions after entrapment, because of the asymmetric distribution and wide range of the homogenisation temperatures (Fig. 11). The above phenomenon is frequently observed in fragile minerals, like calcite. In this particular case, it is possible to specify not only the trapping temperature but also the pressure during entrapment, using the PIT software (Thiéry et al. 2000, 2002). Thus, the temperature and pressure of the fluid at the time of entrapment could be estimated as 80°C and 85 bar, respectively (Fig. 10). Based on the pressure value obtained from the fluid inclusion study, it is possible to establish the thickness of sediments eroded from above the Upper Triassic limestone at Róka Hill from the latest Early Miocene on. Calculating with hydrostatic pressure conditions, the given 85 bar roughly correspond to 850 m. Therefore, since the real pressure may be slightly higher than the hydrostatic pressure, it can be suggested that the thickness of the eroded sediments was ca. 800 m. The above calculated thickness is in accordance with the 850 m total thickness of the Eocene and Oligocene sediments, known from a borehole (Pm-1) in the Pest side (Alföldi et al. 1968; Fig. 13), where these sediments are not yet stripped by erosion. The mean annual surface temperature in Hungary is 12°C (Dövényi et al. 1983), and the geothermal gradient measured in the surroundings of Budapest and believed to have been increasing with time since the Miocene on is ranging between 30 and 60°C/km (Dövényi and Horváth 1988). Thus, the maximum temperature of the fluid should have been only around 60°C at the given dept if it was heated only by the geothermal gradient (calculating with 60°C/km and 800 m depth). Since fluid inclusion data point to higher temperatures (80°C), an external heating agent or origin of fluids from the deeper part of the crust is required. Therefore, the fluid inclusion data can be considered as confirming the hydrothermal origin of calcite.

Based on the observed mineral paragenesis, the hydrothermal fluid certainly carried elevated concentrations of the following elements: Ca, Ba, F, S (both in oxidised and reduced form), Fe, Sr and very minor amounts of Hg and Cu. The source of Ca and CO_3^{2-} may have been both the pore water of the carbonate host rock and the hydrothermal fluids. Moreover, hydrocarbons must have migrated together with the hydrothermal fluids based on the coexistence of water and petroleum in the studied fluid inclusions of calcite. CO_2 was detected in the aqueous phase trapped together with petroleum within one and the same inclusion. No other gas, not even methane, was detected by IR in the aqueous phase in spite of the fact that methane is the most

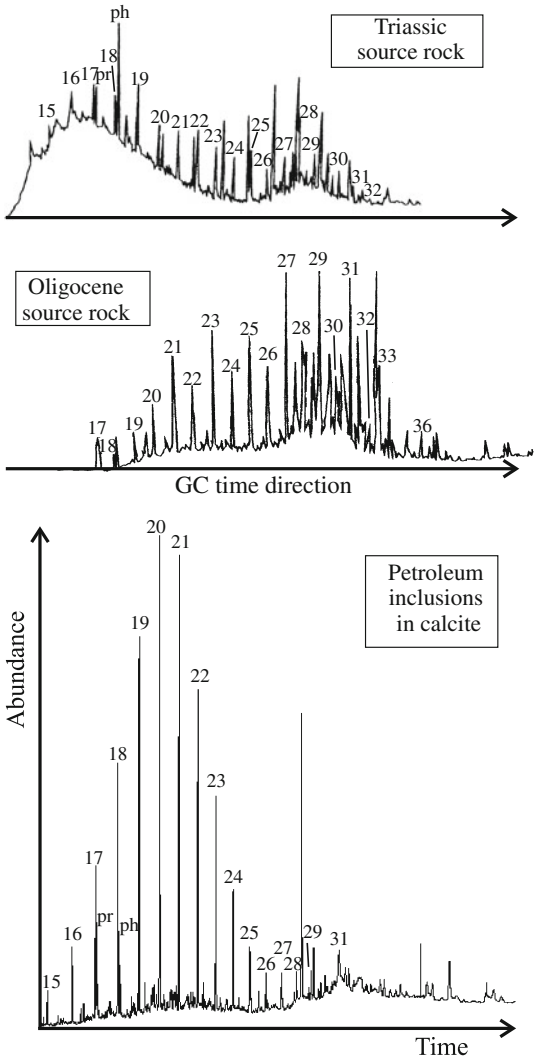

Fig. 12 Gas chromatograms of the extracts of the possible source rocks (Triassic—according to Vető (1999); Oligocene—according to Brukner-Wein et al. (1990)) and of the bulk sample of the petroleum inclusions enclosed in calcite. Carbon atomic number of identified normal alkanes is indicated. *pr* pristane, *ph* phytane

soluble hydrocarbon in water (Guillaume et al. 2003). Nevertheless, in the case of contemporaneous trapping of petroleum and aqueous inclusions, methane saturation is assumed for the aqueous inclusions (Munz 2001). Even though oil always contains some water if they were trapped together (Pironon et al. 2000), we did not detect any water in the petroleum phase. Therefore, it is very likely that the water in the petroleum and the methane in the aqueous phase are present but remain below detection limit. Thus, the aqueous phase, enclosed by the calcite, may represent the H_2O–NaCl–$CH_4 \pm CO_2$–system.

Comparing our results with the fluid inclusion data from barite-II (Gál et al. 2008), a change in the salinity of the hydrothermal fluid can be detected from the calcite towards barite-II (Fig. 11). Calcite is of 0–1.7 wt% salinity which slightly rises in the case of barite-II up to 0.9–2.9 wt%. The very low salinity of the inclusions in calcite may refer to significant karst water contribution to the mineralising fluids. In the case of barite precipitation, the proportion of the mineralising fluids (which is supposed to be more saline than the karst water) might have slightly increased at the expense of the karst water. It has to be emphasised that the very low salinity values suggest that these hydrothermal fluids are the mixture of large amount of warm, regional karst water and small amounts hydrocarbon-bearing fluids of higher salinity.

Hydrocarbons accompanying the hydrothermal fluids can be interpreted as black oil because of the yellow (rarely brown) colour and the high liquid/vapour ratio of individual inclusions at room temperature (Munz 2001). Homogenisation temperature values (around 80°C), the relatively low CH_4-content (<30%) and the high CH_2/CH_3 ratio (~6) are also characteristic to black oils (Grimmer et al. 2003) and point to the presence of long hydrocarbon chains. The commonly detected, visually determined bright bluish-white fluorescence of the petroleum inclusions is not in agreement with the previous statements since this colour is rather characteristic to relatively mature, volatile oils. Although the fluorescence colour of the oil is not only the function of the degree of maturity but it is also affected by the type and origin of source-rock and of course the choice of barrier filters used for fluorescence microscopy. In addition, fluorescence and API gravity variation can reflect maturity but spectrometric colour determination is needed (Oxtoby 2002).

It has been already described that a mixture of petroleum and water provides for a reducing micro-environment in siliciclastic host rock (Surdam et al. 1993). Therefore, it can be suggested that the hydrocarbon-bearing hydrothermal fluid in our case was reducing supported by the following observations: (1) redox front along a calcite vein in the reddish marl (Fig. 4b). (2) presence of sulphides besides the sulphate phases in the same paragenesis where petroleum was found. According to our petrographic observations, those growth zones which contain abundant petroleum inclusions show the brightest cathodoluminescence. Moreover, sector zoning was also observed, showing brighter luminescence where HC-bearing inclusions occurred (Fig. 5c). Recrystallisation of calcite during the moving of aqueous inclusions may explain the above luminescent pattern. Not only the CL pattern of calcites with hydrocarbon inclusions is different from the inclusion-free crystals, but there is a difference in the REE concentrations as well. Those calcite samples, containing petroleum inclusions, are more depleted in REE as compared to those calcite samples without any hydrocarbons (Fig. 9). This trend may refer to the strong sensitivity of the behaviour of REEs to the variation in redox state which might have changed significantly due to the presence of the hydrocarbons. Alternative

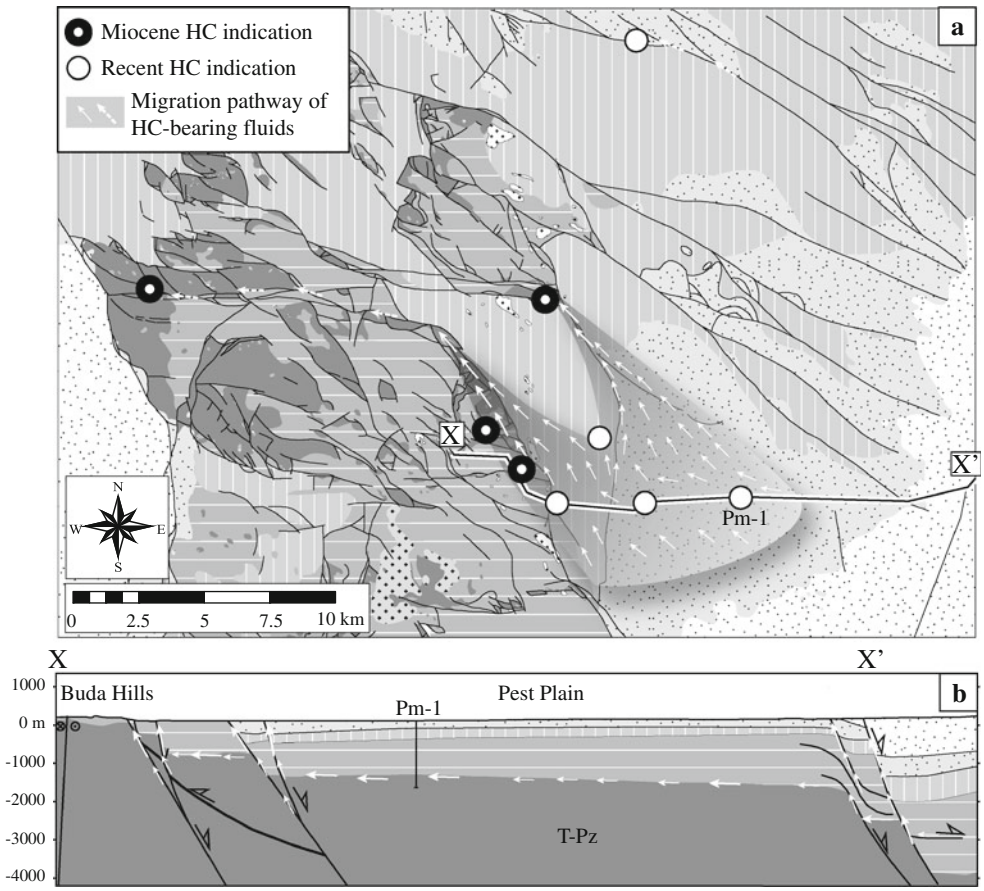

Fig. 13 **a** Miocene and recent HC indications and the reconstructed migration pathway of HC-bearing basinal fluids indicated on the map modified after Fodor (unpublished; detail of Fig. 2). Miocene HC indications include both petroleum inclusions in calcite and stylolite filled with asphalt-like bitumen. Recent HC indications found in groundwater from wells according to Alföldi (1979) **b** Migration pathway indicated on the cross-section modified after Fodor (unpublished). Legend is identical to that of Fig. 2 in the case of both (**a**) and (**b**) figures

explanation is that organic complexation of the REE (e.g. Landström and Tullborg 1995) may have resulted in the depletion of REE in the aqueous phase of the fluid. REE could have been incorporated, however, into calcite in the immediate vicinity of the oil inclusions resulting in the observed more intense luminescence in such places. Thus, the calcite, being precipitated from the aqueous phase migrating together with oil drops, is characterised by overall lower REE content. Although we cannot give the precise explanation for this trend, it is possible to predict whether the calcite likely contains petroleum-bearing inclusions or not based on the REE content of it.

Nevertheless, physical and chemical properties of the hydrothermal fluids may have changed due to the fluid–rock interaction in different host rocks. For example, the absence of the otherwise omnipresent calcite and fluorite in the sandstone may be explained by the changes in the pH of the fluid when entering the pore space of the sandstone or by the lack of the source of the Ca.

Source of the mineralising fluids and the related hydrocarbons

To produce such an extensive hydrothermal mineralisation, it demands a large volume of circulating fluids driven by the elevated heat flux. The question could be raised whether these fluids need a direct volcanic heat source—as it was previously supposed—or not. When accepting the idea of direct volcanic connections, the Visegrád Mts., the closest Neogene volcanic area, north to the Buda Hills, could be considered as the fluid source. However, when we abandon the hypothesis of direct volcanic heat source, hydrocarbon indications may help us to reconstruct the migration pathway by localising the source of the hydrocarbons. There are two possible source rocks in this case, namely the Upper Triassic bituminous limestone and dolomite called Mátyáshegy Formation (Vető 1999) and the Lower Oligocene Tard Clay (Csíky 1956).

Both possible source rocks were investigated with GC by earlier authors (i.e. Brukner-Wein et al. 1990; Vető 1999; Hetényi et al. 2004). In the case of Triassic source rock, there is always a prominent hump between C_{15} and C_{20} on the gas chromatogram (Vető 1999; Hetényi et al. 2004). While the extract of the Tard Clay has always a hump in the C_{27}–C_{32} interval (Brukner-Wein et al. 1990), which may be also present in the case of the Triassic carbonate. The gas chromatogram of our sample (bulk sample of the petroleum inclusions enclosed in the calcite from Róka Hill) shows greater similarities with that of the Tard Clay compared to the other candidate based on the position

of the hump occurring between the C_{27} and C_{32} intervals, confirmed by the lack of the hump between C_{15} and C_{20} characteristics to the Triassic rock (Fig. 12). Moreover, the extremely low pristane/phytane ratio of the Triassic source significantly differs from that observed in our case. Nevertheless, some differences do occur between Oligocene rock and our sample, too, e.g., the normal alkane distribution: (1) The most frequent normal alkane fraction (nC_{27} to nC_{31}) of the Tard Clay extract is of very low concentration in our case. (2) Tard Clay is characterised by odd-predominance which is not obvious in our case. Latter can be explained by the differences in state of maturity since the odd-predominance is an immature character. Lack of high amounts of heavy normal alkanes in our petroleum inclusions may refer the changes in composition of hydrocarbons while being transported by aqueous media. Therefore, we assume that Tard Clay is more likely the source rock in our case than the Triassic bituminous carbonate. Nevertheless, Tard Clay is immature in the whole area of the Buda Hills based on vitrinite reflectance data (Ro = 0.3–0.5%; Korpás et al. 1993). In addition, Tard Clay is immature even at 600–700 depth below ground surface in borehole Ad-3 (Fig. 1b) south-west to Buda Hills ($T_{max} < 430$°C; Brukner-Wein et al. 1990). Therefore, hydrocarbons found as fluid inclusions in the Buda Hills must have been generated from the Tard Clay east to Buda Hills, i.e., under the Pest Plain (Fig. 13) where several known HC accumulations have been reported (e.g. at borehole Gomba-6 where Tard Clay is known from more than 2,000 m depth). Therefore, it can be stated that the mineralising fluids and thus also the associated elements, i.e., Ba, F, S, Fe, Sr, Hg, Cu and hydrocarbons with CO_2 all originated in the basin which borders the Buda Hills from the east. The supposed source of the Ca^{2+} and CO_3^{2-} to precipitate calcite is the karst water. Therefore, we assume that the vein-filling minerals precipitated from a mixture of two fluids, i.e., karst water and basinal water.

Structural control of HC-bearing basinal fluid migration

General strike of the above-described hydrothermal veins (NNW–SSE) is parallel to one of the major structural elements in the Buda Hills, the so-called Solymár Trough (Fig. 2) which is bordered by two normal fault zones formed in the Miocene–Pliocene, due to the predominantly extensional stress field (Fodor et al. 1994). Integrated paleomagnetic and structural studies in the TR revealed several counterclockwise rotation events during Tertiary times (Márton and Fodor 2003). Counterclockwise rotation of the TR resulted in clockwise rotation in the observed stress field. Thus, the strike of the extensional fractures gradually changed from ESE–WNW to NNE–SSW from the Early to Late Miocene (between 19 and 10 Ma). This model thus makes it possible to roughly date different set of veins based on their strike directions. Based on the uniform NNW–SSE strike of the studied veins, the maximum age of the fracturing is latest Early Miocene (17–16 Ma), so the age of the first phase of fracture-filling minerals must be either coeval with or slightly younger than that.

Hydrocarbon indications are all related to these major Miocene–Pliocene faults, indicating that hydrocarbons, just as the hydrothermal fluids, must have migrated mainly along these very faults (Fig. 13a). In addition, the unconformity between Triassic and Eocene carbonates might have also acted as a migration pathway (Milota et al. 1995; Fig. 13b). Hydrocarbon indications in recent groundwater, detected by GC (Alföldi 1979), were found along or near those faults where the Miocene hydrocarbon indications were found (Fig. 13a, b). This implies that basinal fluids, transporting also the hydrocarbons, must have been migrating upward and north-westward to the Buda Karst, using the same migration pathways from the Miocene up to the Holocene and even at present. Evidence for the basinal contribution to the karst system having been active also in post-Miocene times is the presence of barite and fluorite in Pleistocene travertines (Kovács-Pálffy and Földvári 2004) located along the same Miocene–Pliocene faults (Fig. 2). In addition, a less than ca. 1.5 million years old barite-calcite vein is exposed by the Molnár János Cave (Leél-Őssy 2004). Nevertheless, the driving force of the basinal contribution might have changed since the latest Early Miocene. Initially, in the Miocene, due to extension and general subsidence of the Pannonian Basin, a predominantly compaction-driven upward flow is hypothesised, whereas from the Pliocene on, due to the inversion of the Pannonian Basin (Bada et al. 2007) compaction-driven flow must have been converted into a compressional flow (Tóth and Almási 2001).

Hydrocarbon maturation

The source rock of the hydrocarbons is probably the Oligocene Tard Clay. Based on the established age of the petroleum inclusion-bearing calcite veins, we assume that this source rock begun to generate hydrocarbons in the latest Early–Middle Miocene times (~17–11 M years ago). This contradicts to previous estimates by several authors (e.g. Milota et al. 1995) who suggested that the earliest date when this source rock begun to generate hydrocarbons was 6 million years ago. Therefore, it is very likely that HC was generated by forced maturation (sensu Davis and Smith 2006) due to the locally increased heat flux on the margin of the uplifted block because of the continuous upward migration of hydrothermal fluids from the basin. This explains that hydrocarbons were generated

as early as the latest Early–Middle Miocene age here, since the heat that the upward migrating fluids transport by advection and conduction may result in a non-burial organic maturation (Anderson 1991). Nevertheless, forced maturation must have been followed by burial maturation in the subsiding basin. Therefore, recent hydrocarbon indications detected in the wells represent the hydrocarbons generated during burial maturation. Accordingly, the elevated methane content of recent hydrocarbon indications points to the more advanced state of the maturity as compared to Miocene hydrocarbons.

Effect of the basinal contribution to the karst system and to the recent hydrogeological setting

Close spatial relationship between the Miocene hydrothermal veins and the young caves suggests that Miocene hydrothermal fluids have been migrating along the same fractures as the cave-forming fluids; thus, the effect of basinal fluids on the formation of hypogenic caves should be discussed. We suggest that the thermal component of the recent karst is a mixture of regional karst water and hydrocarbon-bearing basinal fluids. Together with the liquid hydrocarbons, aggressive gases (CO_2 and H_2S) have been migrating up to the karst system possibly enhancing the dissolution of carbonates. Methane may also contribute to carbonate dissolution when it is oxidised to CO_2 and H_2O by reaching shallower depths of the aquifer (Forti et al. 2002). However, the proportion of the basinal fluids and also the amount of aggressive gases must have diminished with time in favour of karst water due to accelerating uplift and erosion, as it was suggested already by Schréter (1912).

Summary

Based on detailed mineralogical and fluid inclusion studies, the contribution of hydrocarbon-bearing basinal fluids was proved in the Buda Karst. Our research revealed that the fluid source is the siliciclastic sediment fill of the nearby basin, as it was already suggested in the case of recent thermal water by Alföldi (1979).

Direct volcanic contribution to the hydrothermal fluids could not be confirmed. Instead, the elevated heat flux related to the attenuated lithosphere of the Pannonian Basin should be considered as the heat source of the hydrothermal fluids.

Migration pathways reconstructed for basinal fluids in Miocene times proved to be identical to those of the recent groundwater flow system. It is suggested that basinal contribution has been continuous from the Miocene on. Therefore, hydrothermal events having resulted in the formation of the studied vein-filling minerals, travertines and hypogenic caves should be treated as different phases of the evolution of one single hydrothermal system.

Coexistence of aqueous and petroleum inclusions allowed us to establish the thickness of sediments having been eroded since the latest Early Miocene (800 m) calculated from the entrapment pressure value (85 bar). These data confirm that basinal fluid circulation started under confined conditions as it was suggested by Kovács and Müller (1980). Entrapment temperature (80°C) was also determined and falls within the lower interval of those homogenisation temperature ranges presented in several previous studies from the Buda Hills. It shows that fluid inclusions characterised by extremely high homogenisation temperature values (up to 250°C) should be reconsidered and treated as stretched inclusions.

Extreme low salinity of the fluid inclusions (<1.7 NaCl eq. wt%) implies that basinal fluids were diluted by large amount of regional karst water already in the basin side.

Detailed fluid inclusion studies revealed that significant amounts of CO_2 and minor CH_4 are associated with the black oil-type hydrocarbons migrating upwards from the basin dispersed in an aqueous medium. Unique shape of the petroleum inclusions reconstructed by using CSLM may be the result of separation of water from the inclusion after entrapment, a process known as transcrystalline fluid migration.

Geochemistry of the vein-filling calcite reflects the relatively high temperature origin of the basinal fluids by its significantly depleted oxygen isotopic composition (from −9.2 to −18.7‰). REE concentration of calcite seems to reflect the variable amounts of hydrocarbons present in different samples since those calcites containing abundant petroleum inclusions are depleted in REE as compared to the hydrocarbon-free samples.

Conclusions

Basinal contribution, even if represented by very small amounts, may have several imprints and effects on the karst systems. In the case of the Buda Karst the following effects were detected:

1. Formation of a regional vein-filling paragenesis consisting of calcite, barite, fluorite and sulphide phases.
2. Elevated heat flow, along the margins of the basin possibly resulting in forced maturation of organic-rich sediments. HC inclusions are pointing to maturation of Oligocene source rocks preceding overall burial-related maturation in the basin.
3. Formation of hypogenic caves, not only due to the mixing of different fluids but also due to the dissolution-enhancing effect of aggressive gases (e.g. CO_2 and H_2S), transported upwards from the basin side.

A calcite-barite-fluorite paragenesis, containing hydrocarbon inclusions, associated with sulphides can be considered as a strong indication for basinal contribution in karst water flow systems. In addition, this study provides a clue to estimate the duration of similar flow systems: basinal contribution towards an uplifted block may be maintained for more than 10 M years.

Acknowledgments Financial support for the project was provided by ENI S.p.A. We appreciate the thoughtful discussions with Anita Erőss and Judit Mádl-Szőnyi about the hydrogeology and with László Fodor about the structural geology of the area. We are grateful to Csanád Sajgó for the discussion about the organic geochemical part of the work. We thank the help of Kornél Torkos at the initial stage of gas chromatographic measurements. Márta Berkesi and Tibor Guzmics are acknowledged for their help in Raman analysis. We are thankful to Ádám Vadas and Benedek Gál for their help in the modification of the geological map and cross-section. We appreciate the work of the anonymous reviewer.

References

Alföldi L (1979) Thermal waters of Budapest (in Hungarian). VITUKI Közl 20:1–102

Alföldi L, Bélteky L, Böcker T, Horváth J, Korim K, Liebe P, Rémi R (1968) Thermal waters of Budapest (in Hungarian). VITUKI, Budapest

Anderson GM (1991) Organic maturation and ore precipitation in Southeast Missouri. Econ Geol 86:909–926

Bada G, Horváth F, Dövényi P, Szafián P, Windhoffer G, Cloetingh S (2007) Present-day stress field and tectonic inversion in the Pannonian basin. Glob Planet Change 58:65–180

Báldi T, Nagymarosy A (1976) Silicification of Hárshegy Sandstone and its hydrothermal origin (in Hungarian). Földt Közlöny 106:257–275

Benkovics L, Obert D, Bergerat F, Mansyc JL, Dubois M (1999) Brittle tectonics and major dextral strike-slip zone in the Buda karst (Budapest, Hungary). Geodin Acta (Paris) 12:201–211

Braun G (1889) Minerals of the Buda Hills focusing on calcite (in Hungarian). Pallas Részv társ Ny, Budapest

Brukner-Wein A, Hetényi M, Vető I (1990) Organic geochemistry of an anoxic cycle: a case history from the Oligocene section, Hungary. Org Geochem 15:123–130

Brummer E (1936) Minerals from the quarries of Mátyás-hegy (in Hungarian). Földt Értesítő 1:52–58

Burruss RC (1981) Hydrocarbon fluid inclusions in studies of sedimentary diagenesis. In: Hollister LS, Crawford ML (eds) Short course in fluid inclusions: applications to petrology. Min Assoc Can, Calgary, pp 138–156

Craig H (1965) The measurements of oxygen isotope paleotemperatures. In: Tongiorgi E (ed) Stable isotopes in oceanographic studies and paleotemperatures. Spoleto, Cons Naz Rech, Lab Geol Nucl, Pisa, pp 161–182

Csíky G (1956) Results of the hydrocarbon exploration in the surroundings of Budapest (in Hungarian). Földt Közlöny 86:373–389

Davis GR, Smith LB (2006) Structurally controlled hydrothermal dolomite reservoir facies: an overview. AAPG Bull 90:1641–1690

Dövényi P, Horváth F (1988) A review of temperature, thermal conductivity, and heat flow data from the Pannonian Basin. In: Royden LH, Horváth F (ed) The pannonian basin—a study in basin evolution. AAPG Memoir 45, Tulsa, Okl, pp 195–233

Dövényi P, Horváth F, Liebe P, Gálfi J, Erki I (1983) Geothermal conditions of Hungary. Geophys Trans 29:3–114

Dublyanszky JV (1991) Hydrothermal paleokarst of the Buda Hills. First results of the fluid inclusion studies (in Hungarian). Karszt és Barlang 1–2:9–25

Erőss A, Mádl-Szőnyi J, Csoma ÉA (2008) Characteristics of discharge at Rose and Gellért Hills, Budapest, Hungary. Centr Eur Geol 51:267–281

Fodor L, Magyari Á, Fogarasi A, Palotás K (1994) Tertiary tectonics and late Palaeogene sedimentation in the Buda Hills, Hungary. A new interpretation of the Buda Line. Földt Közlöny 124:129–305

Forti P, Galdenzi S, Sarbu SM (2002) The hypogenic caves: a powerful tool for the study of seeps and their environmental effects. Cont Shelf Res 22:2373–2386

Gál B, Poros Zs, Molnár F (2008) Hydrothermal events in the Hárshegy Sandstone Formation and their relationships to regional geological processes, Buda Hills, Hungary (in Hungarian with English abstract). Földt Közlöny 138:49–60

Gatter I (1984) Fluid inclusion studies of vein-filling minerals in carbonates and the hydrothermal precipitations of the caves (in Hungarian). Karszt és Barlang 1:9–18

Goldscheider N, Mádl-Szőnyi J, Erőss A, Schill E (2010) Review: thermal water resources in carbonate rock aquifers. Hydrogeol J 18:1303–1318

Grimmer JOW, Pironon J, Teinturier S, Mutterer J (2003) Recognition and differentiation of gas condensates and other oil types using microthermometry of petroleum inclusions. Abstract. J Geochem Explor 78–79:367–371

Guillaume D, Teinturier S, Dubessy J, Pironon J (2003) Calibration of methane analysis by Raman spectroscopy in H_2O–NaCl–CH_4 fluid inclusions. Chem Geol 194:41–49

Haas J, Kovács S, Krystyn L, Lein R (1995) Significance of Late Permian—Triassic facies zones in terrain reconstruction in the Alpine-North Pannonian domain. Tectonophys 242:19–40

Hedenquist JW, Henley RW (1985) The importance of CO_2 on freezing point measurements of fluid inclusions: evidence from active geothermal systems and implications for epithermal ore deposition. Econ Geol 80:1379–1406

Hetényi M, Sajgó Cs, Vető I, Brukner-Wein A, Szántó Zs (2004) Organic matter in a low productivity anoxic intraplatform basin in the Triassic Tethys. Org Geochem 35:1201–1219

Klimchouk AB (2007) Hypogene speleogenesis: hydrogeological and morphogenetic perspective. Special Paper no. 1, National Cave and Karst Research Institute, Carlsbad, NM

Korpás L et al (1993) The composite palaeokarst systems of the Buda Hills. Res Rep Geol Inst Hung, Budapest

Kovács J, Müller P (1980) Evolution and evidence of the thermal water activity in the Buda Hills (in Hungarian). Karszt és Barlang 2:93–98

Kovács-Pálffy P, Földvári M (2004) Mineralogy of the travertines in NE Transdanubia (Hungary). Földt Közlöny 134:563–587

Landström O, Tullborg EL (1995) Interactions of trace elements with fracture filling minerals from the Äspö Hars Rock laboratory. SKB Techn Rep TR 95–13. Swed Nucl Fuel and Waste Management Co. (SKB), Stockholm

Leél-Őssy Sz (2004) Genesis and values of hydrothermal caves in the Buda Hills (in Hungarian). In: Hazslinszky T (ed) Genesis and formations of hydrothermal caves. Proceedings on International Conference on the occasion of the 100th anniversary of the discovery of the Pál-völgy Cave, Budapest, Hung Speleol Soc, pp 45–53

Leél-Őssy Sz, Surányi G (2003) Peculiar hydrothermal caves in Budapest, Hungary. Acta Geol Hung 46:407–436

Lemmlein GG (1952) Migration of liquid fluid inclusions in a crystal towards a source of heat. Dokl Akad Nauk SSSR 85:325–328
Lenkey L, Dövényi P, Horváth F, Cloetingh SAPL (2002) Geothermics of the Pannonian basin and its bearing on the neotectonics. EGU Stephan Mueller Spec Publ Ser 3:29–40
Lóránth Cs (2000) Copper in the Buda Hills (in Hungarian). AuXit 2:28–29
Márton E, Fodor L (2003) Tertiary paleomagnetic results and structural analyses from the Transdanubian Range (Hungary): rotational disintegration of the ALCAPA unit. Tectonophys 363:201–224
McCrea JM (1950) On the isotopic chemistry of carbonates and a paleotemperature scale. J Chem Phys 18:849–857
Milota K, Kovács A, Galicz Zs (1995) Petroleum potential of the North Hungarian Oligocene sediments. Petrol Geosci 1:81–87
Molnár F, Gatter I (1994) Comparative mineralogic-genetic studies of sedimentary and hydrothermal barite crystals from Hungary. Földt Közlöny 124:43–57
Müller P, Magyar I (2008) The Pannonian deposits of the Buda Mountains (in Hungarian with English abstract). Földt Közlöny 138:345–356
Munz IA (2001) Petroleum inclusions in sedimentary basins: systematics, analytical methods and applications. Lithos 55:195–212
Nádor A (1991) Paleokarstic features of the Buda Hills and their evolution (in Hungarian). Ph.D. Dissertation, Eötvös L. University, Budapest
Nádor A (1992) Paleokarstic features in Triassic-Eocene carbonates. Zent Blatt Geol Palentol 1:1317–1329
Nagy B, Pelikán P (1976) Metacinnabar and cinnabar from the Róka Hill (in Hungarian). Ann Rep Geol Inst Hung of 1973, pp 51–55
Nedkvitne T, Karlsen DA, Bjørlykke K, Larter S (1993) Relationship between reservoir diagenetic evolution and petroleum emplacement in the Ula field, North Sea. Mar Petrol Geol 10:255–270
Oxtoby NH (2002) Comments on: assessing the maturity of oil trapped in fluid inclusions using molecular geochemistry data and visually-determined fluorescence colours. Critical comment. Appl Geochem 17:1371–1374
Pironon J, Thiéry R, Teinturier S, Walgenwitz F (2000) Water in petroleum inclusions: evidence from Raman and FT-IR measurements, PVT consequences. J Geochem Explor 69–70:663–668
Royden LH, Horváth F (1988) The Pannonian basin—a study in basin evolution. AAPG Memoir 45, Tulsa, Okl
Schafarzik F (1921) Retrospection of the evolution of thermal springs in Buda (in Hungarian). Hidrol Közlöny 1:9–14
Scheuer Gy, Schweitzer F (1988) Travertines of the Gerecse and Buda Mountains (in Hungarian). Földr Tanulm 20, Akadémai Kiadó, Budapest
Schréter Z (1912) The evolution of thermal springs in Buda (in Hungarian). Magy Balneol Értesítő 1:2–4
Surdam RC, Jiao ZS, MacGowan DB (1993) Redox reactions involving hydrocarbons and mineral oxidants, a mechanism for significant porosity enhancement in sandstones. AAPG Bull 77:1509–1518
Takács-Bolner K, Kraus S (1989) Results of research of thermal water caves (in Hungarian). Karszt és Barlang 1–2:61–66
Tari G (1994) Alpine Tectonics of the Pannonian Basin. Ph.D. Dissertation, Rice University, TX
Taylor SR, McLennan SM (1985) The continental crust: its composition and evolution. Blackwell, Oxford
Thiéry R, Pironon J, Walgenwitz F, Montel F (2000) PIT (Petroleum Inclusion Thermodynamic): a new modelling tool for the characterization of hydrocarbon fluid inclusions from volumetric and microthermometric measurements. J Geochem Explor 69–70:701–704
Thiéry R, Pironon J, Walgenwitz F, Montel F (2002) Individual characterization of petroleum inclusions (composition and P-T trapping conditions) by microthermometry and confocal scanning laser microscopy: inferences from applied thermodynamics of oils. Mar Petrol Geol 19:847–859
Tóth J, Almási I (2001) Interpretation of observed fluid potential patterns in a deep sedimentary basin under tectonic compression: Hungarian Great Plain, Pannonian Basin. Geofluids 1:11–36
Tullborg EL, Drake H, Sandström B (2008) Palaeohydrogeology: a methodology based on fracture mineral studies. Appl Geochem 23:1881–1897
Vető I (1999) Triassic sourced oil shows near Budapest. Ann Rep Geol Inst Hung of 1992–1993 vol 2, pp 111–115
Wein Gy (1977) Tectonics of the Buda Hills (in Hungarian). Spec Publ Geol Inst Hung, Budapest